

Chapter 3

Diffraction on cylindrical inhomogeneities comparable to the wavelength

In opto- and microelectronics, as well as in nanophotonics use is made of sophisticated optical devices with the dimensions of the order of the wavelength of incident light, whose work is described by the non-trivial physical effects, such as multiple scattering on periodic structures (Bragg diffractive gratings), the scattering and diffraction on aperiodic structures (diffractive optical elements (DOE)), the dispersion and non-linear transformation of laser pulses. The effect of these elements can not be predicted on the basis of geometrical optics or scalar diffraction theory, and it is essential to study the propagation of light waves through them using the vector model of diffraction. All this creates a greater need for efficient numerical approaches for modelling the wave propagation of light, if possible taking into account dispersion, scattering, complex interference effects, etc. Also, the use of the vector diffraction model is required when the relevant calculation area is located near or within the optical element. Although analytical solutions of the vector diffraction problem can be obtained for selected objects (sphere, half-cylinder) [1, 2] the boundary conditions on the electromagnetic field for other dielectric structures makes the analytic solution impossible.

Thus, for the problems of modelling the diffraction of light on the elements with dimensions on the order of the wavelength the light must be regarded as electromagnetic radiation, which allows us to transfer many of the developed methods of electromagnetic simulation of microwave and radio waves to the area of optical modelling.

Most numerical methods (the method of moments, the finite difference method, the boundary element method, the finite element method, etc.) came into optics from other areas of science and so far no universal approach has been developed which would cover a large number of optical (and electromagnetic) problems. In general, it is usually necessary to combine two or three methods to calculate a wide range of problems that lead to the development of various integrated modelling techniques [3–5].

The bulk of the numerical diffraction simulation methods can be classified as differential [32], difference [33, 34], integral [35–38], variational [39–41], the discrete sources [42], and the propagation of rays [43].

In this section, we discuss finite element methods for solving the two-dimensional Helmholtz equation and for the solution of the two-dimensional diffraction integral equation.

3.1 Analysis of diffraction on inhomogeneities by the combined finite element and boundary element method

3.1.1. Analysis of the diffraction of light on non-periodic irregularities

In the problems of modelling the diffraction of light on the optical elements in a homogeneous space with dimensions on the order of the wavelength the light must be regarded as electromagnetic radiation.

To determine the electromagnetic fields at a point of space, integral methods combine the contributions to this point from the field of sources in the volume or on the surface. The popularity of the integral methods is based on their ability to solve unlimited field problems, as the Sommerfeld radiation condition is certainly satisfied in the formulation of the problem. Moreover, the integral methods require knowledge of the field only on the surface of the diffraction element, and not of the total field in a space and this minimizes the number of unknowns. In [21, 22] the authors presented a method based on the combined boundary element method. In [23] a method was developed for calculating the diffraction on a plane-parallel plate with the heterogeneity on the basis of integral equations associated with the numerical solution of the Green tensor. The disadvantage of these methods is that they lead to fully populated matrices and, therefore, require more computer memory and long calculation time. Also, the limit of the application of methods should be chosen at the physical boundary of the object. If the inhomogeneity has a nontrivial form, it leads to an increase in the number of unknowns.

The difference solution of differential Maxwell equations was considered in [7, 24–27]. In [28] the difference solution of the wave equation was described. The disadvantages of this approach are the inability to use the radiation conditions and restrictions on the steps of the grid. To simulate the steady-state problems of passage of radiation by difference schemes, it is necessary to use a finite number of wavelengths of the incident pulse which distorts the wave spectrum. The use of the absorbing boundary conditions [13, 29] as boundary conditions for unbounded diffraction problems allows us to solve approximately the Maxwell's equations by difference schemes and the accuracy of the solution depends on the number of layers on the artificial boundary and the degree of its isolation???

In contrast to the methods of finite difference solution of Maxwell's equations, the integral and variational methods do not require the construction of complex absorbing boundary conditions [13, 18].

Variational methods in problems with a limited range of tasks determine solutions of the Helmholtz equation by minimizing the functional relation. In [13], the Helmholtz equation was solved by the Galerkin finite element method using the

boundary conditions of the complex type that depend on the unknown parameter which required the use of the border of a certain form. In addition, this method also does not include the Sommerfeld radiation conditions.

In [3] the authors presented a hybrid method based on the finite element method, formulated by the Ritz method, and the boundary element method. In this hybrid method the finite element method is used to solve the Helmholtz equation in the inner part of the inhomogeneous dielectric element of micro-optics method and the integral method and the boundary element method are used for the region external to the element where the radiation condition must be satisfied. Both methods are joined at the boundary between inner and outer parts, with the satisfaction of the conditions of continuity of the field. Using the finite element method to determine the field inside the object leads to a tridiagonal matrix, which requires less computer memory and shorter computing time than the methods of the volume integrals [30]. The result of using the boundary element method for determining the field at the boundary is a more accurate solution than using the finite element method with absorbing boundary conditions. But the application of the Ritz method to solve the Helmholtz equation is incorrect because it imposes a requirement of the positivity of the operator of the equation being solved. No conclusion can be made on the definite sign of the operator of the Helmholtz equation.

Description of the method of calculation

In this problem, a source in space illuminates a cylindrical structure. In the absence of the structure the source of the incident field. In the presence of the structure this source creates another field, called the total field. The scattered field is defined as the difference between the total field and the incident field. The purpose of the task is to determine the total or scattered field, characterizing the structure.

Any two-dimensional field can be decomposed into E_z -polarized and H_z -polarized fields. In the diffraction domain the field is described by a system of differential equations for various cases of TE- and TM-polarizations. For TE-polarization ($\mathbf{E}(x,y) = (0,0, E_z(x, y))$) the complex amplitude $u(x, y)$ denotes the total electric field $E_z(x, y)$, which is directed along the axis z (along the generatrix of a cylindrical optical element), the coordinates (x,y) lie in the plane of the normal section. For the TM-polarization ($\mathbf{H}(x,y) = (0,0, H_z(x, y))$) the complex amplitude $u(x, y)$ denotes the total magnetic field $H_z(x, y)$.

The total field $u_\Omega(x, y)$ in the Ω region must satisfy the equation

$$\nabla \cdot \left[\frac{1}{p(x,y)} \nabla u_\Omega(x, y) \right] + k_0^2 q(x,y) u_\Omega(x, y) = f_\Omega, \quad (3.1)$$

where $f_\Omega = jk_0 Z_0 J_z$, $p(x,y) = \mu_r$, $q(x, y) = \varepsilon_r$ for TE polarization, and

$$f_\Omega = -\frac{\partial}{\partial x} \left(\frac{1}{\varepsilon_r} J_y \right) + \frac{\partial}{\partial y} \left(\frac{1}{\varepsilon_r} J_x \right), p(x,y) = \mu_r, q(x,y) = \varepsilon_r$$

for TM polarization. Constants m_r and e_r is the ratio

of magnetic and dielectric constants of the medium to the same performance space, i.e. $\mu_r = \mu/\mu_0$ and $\varepsilon_r = \varepsilon/\varepsilon_0$, k_0 is the wave number of waves in free space

$$k_0 = \omega(\mu_0\varepsilon_0)^{1/2} = \frac{\omega}{c} = \frac{2\pi}{\lambda_0}, \quad (3.2)$$

$Z_0 = \sqrt{\mu_0/\varepsilon_0}$ is the impedance of free space, J is the density of the electric current source.

In this problem the calculation domain is infinite. However, as is known, the finite element method (FEM) is applicable only to a finite or limited area. Thus, to solve the equation (3.1), an infinite domain Ψ , external to the scatterer, should be limited by the introduction of the artificial boundary Γ . Correspondingly, for the only solution of the problem, boundary conditions must be imposed at this artificial boundary. Such conditions should make the border transparent as possible for the scattered field or, in other words, minimize the non-physical reflections from the boundary. One of the classes of the boundary conditions, designed for this purpose, can be obtained from the boundary integral equations applied to the outer region. These boundary conditions are global in nature, i.e. they relate to the field at a boundary node with the field across the boundary. These boundary conditions prevent reflection at the boundary for all angles of incidence of the waves and lead to the exact solution.

Thus, it is necessary to define the total field $u(x, y)$ in the domains Ω (internal) and Ψ (external) satisfying the above conditions.

Galerkin's solution of equation (1) is based on solving the relations of the form:

$$\iint_{\Omega} \left(-\frac{1}{p} \Delta u_{\Omega} \gamma - qk^2 u_{\Omega} \gamma - f_{\Omega} \gamma \right) d\Omega = 0. \quad (3.3)$$

where γ is an arbitrary function from the domain of equation (1).

Using the first Green's formula:

$$\iint_{\Omega} P \Delta Q d\Omega = \int_{\Gamma} P \frac{dQ}{dn} dl - \iint_{\Omega} \nabla P \nabla Q d\Omega,$$

for the functions P and Q , where Ω is the domain of the plane x, y ; Γ is its boundary, required anti-clockwise $\frac{dQ}{dn}$ - the derivative in the direction of the outward normal to the curve Γ , we obtain:

$$\iint_{\Omega} \left(\frac{1}{p} \nabla u_{\Omega}(x, y) \nabla \gamma - qk^2 u_{\Omega}(x, y) \gamma \right) d\Omega - \int_{\Gamma} \frac{\gamma}{p} \frac{du_{\Omega}(x, y)}{dn} d\Gamma = \iint_{\Omega} f_{\Omega} \gamma d\Omega. \quad (3.4)$$

System of basis functions for Ω denote $\left\{ \omega_{k,l}^{\Omega}(x, y) \right\}_{k,l=0}^{N_x, N_y}$ and the system of basis functions for Γ denote $\left\{ \omega_m^{\Gamma}(x, y) \right\}_{m=1}^M$, where N_x, N_y is the number of nodes of the grid covering a rectangular area Ω on the x and y axis, respectively, M - number of nodes of the grid covering the boundary Γ .

Replacing in (3.4) the arbitrary function γ by the system of basis functions for Galerkin's method, we can write the system of linear equations:

$$\mathbf{A}u + \mathbf{B}v = \mathbf{C}f, \quad (3.5)$$

where $u = (u_1, \dots, u_{N_x N_y})^T$ is the vector consisting of coefficients

$\{u_{N_y(k)+l} = u_{k,l}\}_{k,l=0}^{N_x, N_y}$ of the expansion:

$$u^\Omega(x, y) = \sum_{k,l=0}^{N_x, N_y} u_{k,l} \omega_{k,l}^\Omega(x, y). \quad (3.6)$$

The vector $f = (f_1, \dots, f_{N_x N_y})^T$ is the vector consisting of the coefficients of the expansion:

$$f^\Omega(x, y) = \sum_{k,l=0}^{N_x, N_y} f_{k,l} \omega_{k,l}^\Omega(x, y). \quad (3.7)$$

Although (3.6) and (3.7) are valid for all points (x, y) in the domain Ω , it is necessary to process separately the values of the field and its partial derivatives on the boundary Γ from the values in the inner region. The decomposition, similar to (3.6) and (3.7), for the field and its partial derivatives at the boundary has the form:

$$u^\Gamma(x, y) = \sum_{m=1}^M u_m \omega_m^\Gamma(x, y), \quad (3.8)$$

$$v^\Gamma(x, y) = \sum_{m=1}^M v_m \omega_m^\Gamma(x, y), \quad (3.9)$$

$$f^\Gamma(x, y) = \sum_{m=1}^M f_m \omega_m^\Gamma(x, y), \quad (3.10)$$

where $(x, y) \in \Gamma$, $v = (v_1, \dots, v_M)^T$ is the vector consisting of the expansion coefficients $v_k = \partial u_k / \partial \mathbf{n}$.

The elements of the matrix \mathbf{A} are calculated from the equations:

$$a_{N_y k+l, N_y i+j} = \iint_{\Omega_{k,l}} \left(\frac{1}{p(x, y)} \left[\frac{\frac{\partial \omega_{k,l}^\Omega(x, y)}{\partial x} \frac{\partial \omega_{i,j}^\Omega(x, y)}{\partial x}}{\frac{\partial \omega_{k,l}^\Omega(x, y)}{\partial y} \frac{\partial \omega_{i,j}^\Omega(x, y)}{\partial y}} + \right] - k_0^2 q(x, y) \omega_{k,l}^\Omega(x, y) \omega_{i,j}^\Omega(x, y) \right) d\Omega, \quad (3.11)$$

$$k, i = [1, N_x], l, j = [1, N_y],$$

where $\Omega_{k,j}$ is the domain of decomposition of domain Ω , consisting of nodes k and j .

The elements of the matrix are given by:

$$b_{m,s} = - \oint_{\Gamma_{m,s}} \omega_m^\Gamma \omega_s^\Gamma dl, \quad (3.12)$$

$$m, s = [1, M],$$

where $\Gamma_{m,s}$ is the linear region of the boundary Γ , which includes the boundary nodes m and s .

The elements of the matrix \mathbf{C} are given by:

$$c_{N_y k+l, N_x i+j} = \iint_{\Omega_{k,l}} \omega_{k,l}^\Omega(x,y) \omega_{i,j}^\Omega(x,y) d\Omega, \quad (3.13)$$

$$k, j = [1, N_x], l, j = [1, N_y],$$

where $\Omega_{k,j}$ is the domain of decomposition of Ω , consisting of nodes k and j .

As a piece-wise linear basis we determine the function of the form:

$$\omega_{k,l}^\Omega(x,y) = \begin{cases} 1 - \frac{x_k - x}{h} - \frac{y_l - y}{h}, & x, y \in \Omega_{k,l,1}^h \\ 1 - \frac{x_k - x}{h}, & x, y \in \Omega_{k,l,2}^h \\ 1 + \frac{y_l - y}{h}, & x, y \in \Omega_{k,l,3}^h \\ 1 + \frac{x_k - x}{h} + \frac{y_l - y}{h}, & x, y \in \Omega_{k,l,4}^h \\ 1 + \frac{x_k - x}{h}, & x, y \in \Omega_{k,l,5}^h \\ 1 - \frac{y_l - y}{h}, & x, y \in \Omega_{k,l,6}^h \end{cases}, \quad (3.14)$$

where h is the length of the segment of the coverage ???.

Elements $(a_{k,l}^{ij})$ of the matrix \mathbf{A} , the elements $(b_{m,s})$ of the matrix \mathbf{B} and elements $(c_{k,l}^{ij})$ of the matrix \mathbf{C} are calculated from equations (3.11) (3.12) and (3.13), respectively. Then, the system of equations (3.5) can be written as:

$$\begin{bmatrix} [\mathbf{A}_{\Omega,\Omega}] & [\mathbf{A}_{\Gamma,\Omega}] & 0 \\ [\mathbf{A}_{\Omega,\Gamma}] & [\mathbf{A}_{\Gamma,\Gamma}] & [\mathbf{B}] \end{bmatrix} \begin{bmatrix} \mathbf{u}_\Omega \\ \mathbf{u}_\Gamma \\ \mathbf{v}_\Gamma \end{bmatrix} = \begin{bmatrix} [\mathbf{C}_{\Omega,\Omega}] & [\mathbf{C}_{\Gamma,\Omega}] \\ [\mathbf{C}_{\Omega,\Gamma}] & [\mathbf{C}_{\Gamma,\Gamma}] \end{bmatrix} \begin{bmatrix} \mathbf{f}_\Omega \\ \mathbf{f}_\Gamma \end{bmatrix}. \quad (3.15)$$

The system of equations (3.15) has no unique solution, since it consists of N equalities with $N + M$ unknowns: $N = N_x N_y$ is the total number of nodes of the

field $u_{k,l}(x, y)$ in the domain Ω and M and derivatives along the normal to the boundary nodes $v_{k,l}(x, y)$.

We define the field in free space Ψ (outside the domain Ω with its boundary Γ). Since this is a homogeneous space, then the field can be formulated in terms of boundary integrals with the appropriate Green's function. The total field $u_\Psi(x, y)$ in domain Ψ must satisfy the following equation:

$$\nabla \cdot \left[\frac{1}{p} \nabla u_\Psi(\xi) \right] + k_0^2 q u_\Psi(\xi) = f_\Psi, \quad \xi \in \Psi, \quad (3.16)$$

where $f_\Psi = jk_0 Z_0 J_z^\Psi$, $p(x, y) = \mu_r$, $q(x, y) = \varepsilon_r$ for TE-polarization and $f_\Psi = -\frac{\partial}{\partial x} \left(\frac{1}{\varepsilon_r} J_y^\Psi \right) + \frac{\partial}{\partial y} \left(\frac{1}{\varepsilon_r} J_x^\Psi \right)$ for TM-polarization, J^y is the density of electric current density in free space.

To construct the boundary integral equation for the field and its normal derivative, we introduce the Green function u^* which satisfies the Sommerfeld radiation condition and is the fundamental solution of the Helmholtz equation:

$$\nabla^2 u^*(\xi, \eta) + k^2 u^*(\xi, \eta) = -\delta(\xi, \eta), \quad \eta \in \Psi. \quad (3.17)$$

The fundamental solution for the Helmholtz equation in the two-dimensional homogeneous space is well known and has the form

$$u^* = (i/4) H_0^{(1)}(kr), \quad (3.18)$$

where

$$r = \sqrt{[x_1(\eta) - x_1(\xi)]^2 + [x_2(\eta) - x_2(\xi)]^2}$$

$H_0^{(1)}(kr) = J_0(kr) + iY_0(kr)$ is the Hankel function of the first kind and zeroth order, where J_0 is the Bessel function of zeroth order, Y_0 is the Neumann function of zeroth order.

To construct the boundary integral equation for the scattered field and its normal derivative, we use Green's theorem as follows:

$$\begin{aligned} & \int_{\Psi} \left[\nabla^2 u^*(\xi, \eta) + k^2 u^*(\xi, \eta) \right] u(\eta) d\Psi = \\ & = - \int_{\Gamma} q(\eta) u^*(\xi, \eta) d\Gamma + \int_{\Gamma} u(\eta) q^*(\xi, \eta) d\Gamma + \int_{\Psi} f_\Psi(\eta) u^*(\xi, \eta) d\Psi. \end{aligned} \quad (3.19)$$

The functions in both integrals on the right side of equation (3.19) $q(\eta) = \partial u(\eta) / \partial \mathbf{n}'$ are the normal derivatives of the field amplitude.

Substituting (3.17) into (3.19) and passing to the limit of the observation point ξ from the inner point to the boundary???, we find

$$c(\xi)u(\xi) = -\int_{\Psi} f_{\Psi}(\eta)u^*(\xi, \eta)d\Psi + \int_{\Gamma} q(\eta)u^*(\xi, \eta)d\Gamma - \int_{\Gamma} u(\eta)q^*(\xi, \eta)d\Gamma. \quad (3.20)$$

This equation provides a functional link between the functions u and their normal derivative q at the boundary Γ . The function c in (3.20) is equal to:

$$c(\xi) = 1 - \frac{1}{2\pi}\phi, \quad (3.21)$$

where ϕ is the interior angle of the piecewise-near boundary at point ξ . The first term on the right side is the field produced by a source f_{Ψ} in free space, and may be designated as the incident field u_{Ψ}^{in} .

Thus, equation (3.20) is written as follows:

$$c(\xi)u(\xi) = \int_{\Gamma} q(\eta)u^*(\xi, \eta)d\Gamma - \int_{\Gamma} u(\eta)q^*(\xi, \eta)d\Gamma + u_{\Psi}^{\text{in}}(\xi). \quad (3.22)$$

Substituting the function of the complex amplitude in equation (3.22) at the boundary by its approximation by basic piecewise-linear functions at $\xi \in \Gamma$ (3.8) and (3.9), we obtain

$$c_m u_m = \sum_{s=1}^M h \left\{ v_s \left[\int_0^1 \omega_s^{\Gamma}(\rho_s + [\rho_{s+1} - \rho_s]\gamma) u^*(\rho_m, \rho_s + [\rho_{s+1} - \rho_s]\gamma) d\gamma + \int_0^1 \omega_s^{\Gamma}(\rho_{s-1} + [\rho_s - \rho_{s-1}]\gamma) u^*(\rho_m, \rho_{s-1} + [\rho_s - \rho_{s-1}]\gamma) d\gamma \right] - u_s \left[\int_0^1 \omega_s^{\Gamma}(\rho_s + [\rho_{s+1} - \rho_s]\gamma) \frac{\partial u^*(\rho_m, \rho_s + [\rho_{s+1} - \rho_s]\gamma)}{\partial \mathbf{n}'} d\gamma + \int_0^1 \omega_s^{\Gamma}(\rho_{s-1} + [\rho_s - \rho_{s-1}]\gamma) \frac{\partial u^*(\rho_m, \rho_{s-1} + [\rho_s - \rho_{s-1}]\gamma)}{\partial \mathbf{n}'} d\gamma \right] \right\} + u_m^{\text{in}}, \quad m = [1, M], \quad (3.23)$$

which can be represented in the matrix form

$$[D] \bar{\mathbf{u}}_{\Gamma} + [G] \bar{\mathbf{v}}_{\Gamma} = \bar{\mathbf{u}}_{\Gamma}^{\text{in}}. \quad (3.24)$$

with elements of the matrices $[D]$ and $[G]$ in the form

$$d_{m,s} = -h \left[\int_0^1 \omega_s^{\Gamma}(\rho_s + [\rho_{s+1} - \rho_s]\gamma) \frac{\partial u^*(\rho_m, \rho_s + [\rho_{s+1} - \rho_s]\gamma)}{\partial \mathbf{n}'} d\gamma + \int_0^1 \omega_s^{\Gamma}(\rho_{s-1} + [\rho_s - \rho_{s-1}]\gamma) \frac{\partial u^*(\rho_m, \rho_{s-1} + [\rho_s - \rho_{s-1}]\gamma)}{\partial \mathbf{n}'} d\gamma \right] - c_m \delta_{ms}, \quad (3.25)$$

$$g_{m,s} = h \left[\int_0^1 \omega_s^\Gamma (\boldsymbol{\rho}_s + [\boldsymbol{\rho}_{s+1} - \boldsymbol{\rho}_s] \gamma) u^* (\boldsymbol{\rho}_m, \boldsymbol{\rho}_s + [\boldsymbol{\rho}_{s+1} - \boldsymbol{\rho}_s] \gamma) d\gamma + \int_0^1 \omega_s^\Gamma (\boldsymbol{\rho}_{s-1} + [\boldsymbol{\rho}_s - \boldsymbol{\rho}_{s-1}] \gamma) u^* (\boldsymbol{\rho}_m, \boldsymbol{\rho}_{s-1} + [\boldsymbol{\rho}_s - \boldsymbol{\rho}_{s-1}] \gamma) d\gamma \right], \quad (3.26)$$

$$m, s = [1, M].$$

The integrals in (3.25) and (3.26) can be evaluated numerically. Combining equations (3.15) and (3.24), we obtain a closed system of linear algebraic equations for solving the problem of diffraction of a plane wave by a cylindrical micro-object

$$\begin{bmatrix} [\mathbf{A}_{\Omega, \Omega}] & [\mathbf{A}_{\Gamma, \Omega}] & \mathbf{0} \\ [\mathbf{A}_{\Omega, \Gamma}] & [\mathbf{A}_{\Gamma, \Gamma}] & [\mathbf{B}] \\ \mathbf{0} & [\mathbf{D}] & [\mathbf{G}] \end{bmatrix} \begin{bmatrix} \mathbf{u}_\Omega \\ \mathbf{u}_\Gamma \\ \mathbf{v}_\Gamma \end{bmatrix} = \begin{bmatrix} [\mathbf{C}_{\Omega, \Omega}] & [\mathbf{C}_{\Gamma, \Omega}] & \mathbf{0} \\ [\mathbf{C}_{\Omega, \Gamma}] & [\mathbf{C}_{\Gamma, \Gamma}] & \mathbf{0} \\ \mathbf{0} & \mathbf{0} & [\mathbf{E}] \end{bmatrix} \begin{bmatrix} \mathbf{f}_\Omega \\ \mathbf{f}_\Gamma \\ \mathbf{u}_\Gamma^{\text{in}} \end{bmatrix}, \quad (3.27)$$

where the submatrix $\mathbf{A}_{\Omega, \Omega}$ with the dimension $(N - M) \times (N - M)$ includes the ratio of the field in the internal nodes of the partition grid, submatrix $\mathbf{A}_{\Omega, \Gamma}$ and $\mathbf{A}_{\Gamma, \Omega}$, with dimension $(N - M) \times M$ and $M \times (N - M)$, respectively, include the coupling coefficients of the field at the boundary and interior nodes, submatrix $\mathbf{A}_{\Gamma, \Gamma}$ with the size $M \times M$ involves the coupling coefficients of the field at the boundary nodes, the submatrix \mathbf{B} with the size $M \times M$ includes the ratios between the derivatives of the field at the boundary of the field and in the internal nodes of the partition grid, submatrix \mathbf{D} with the size $M \times M$ involves the coupling coefficients of the field of free space at the boundary nodes, the \mathbf{G} with the size $M \times M$ includes the ratio between derivatives of the field at the boundary and the field of free space in the internal nodes of the partition grid. Submatrix $\mathbf{C}_{\Gamma, \Gamma}$ with the dimension $(N - M) \times (N - M)$ includes the ratio of field sources in the internal nodes of the partition grid, submatrices $\mathbf{C}_{\Omega, \Gamma}$ and $\mathbf{C}_{\Gamma, \Omega}$ with the dimension $(N - M) \times M$ and $M \times (N - M)$, respectively, include the ratio of field sources in the boundary and internal nodes, the submatrix $\mathbf{C}_{\Gamma, \Gamma}$ with the size $M \times M$ includes the ratio of the field sources at the boundary nodes. Submatrix \mathbf{E} is the identity matrix with the size $M \times M$. Vectors \mathbf{u}_Ω and \mathbf{u}_Γ are the vectors of the strength of the field in the interior and boundary nodes of the grid, \mathbf{v}_Γ is the vector of normal derivatives of the field at the boundary nodes. Vectors \mathbf{f}_Ω and \mathbf{f}_Γ are the vectors of the field sources in the interior and boundary nodes of the grid, u_Γ^{in} is the vector of the strength of the external incident field at the boundary nodes of the grid. Thus, the dimension of the system of equations (3.27) is $(N + M) \times (N + M)$.

After determining the values of the field and its derivatives on the boundary Γ the field at any point of doimain Ψ is defined by (3.22), where $c(\zeta) = 1$.

Examples of calculation

Consider the diffraction of a plane wave (TE- and TM-polarizations) on dielectric and conducting homogeneous cylinders with a circular cross-section for the experimental investigation of convergence of the combined method. The convergence of the algorithm depends on the length of the segment h , the wavelength of the source λ , μ_r and ϵ_r of the medium. Since the magnetic and dielectric constants of the medium are the variables in the problem, we consider the dependence of solutions on the parameter λ/h that determines the number of grid segments on the same wavelength. Let the plane wave falls on the cylinder, the wavelength $\lambda_0 = 0.5 \mu\text{m}$. The radius of the cylinder is $0.25 \mu\text{m}$. The relative dielectric permittivity of the conducting cylinder made of is aluminum $\epsilon = -4.4 + i11.9$. The relative dielectric permittivity of the dielectric cylinder $\epsilon = 2.25$. The parameters of the homogeneous space surrounding the cylinder are $\epsilon = \mu = 1$. The calculation were made by the joint ??? method. Domain Ω was represented by a square region, the contour Γ was the perimeter of domain Ω . No sources were situated inside Ω . Domain Ω was covered with a square grid consisting of 105×105 nodes. The calculation time was 10 min on a PC Pentium 4.

Figure 3.1 shows the results of numerical modelling of diffraction of TE- and TM-waves on a dielectric cylinder. Figure 3.2 shows the simulation results of diffraction on the conducting cylinder.

To evaluate the diffractive processes, we use the directional diagram of scattering, which depends on the angular coordinate φ , as defined at points at infinity $(\rho \rightarrow \infty)$ as

$$\sigma(\varphi) = \lim_{\rho \rightarrow \infty} 2\pi\rho \frac{|u^{sc}|^2}{|u^{in}|^2}. \quad (3.28)$$

In particular, the directional diagram is determined in the forward direction ($\varphi = 0$), in the opposite direction ($\varphi = \pi$) and in the transverse direction ($\varphi = \pi/2$). The following shows the dependence of σ/λ on parameter λ/h . The results are presented in dB ($\sigma_{\text{DB}} = 10 \log_{10} \sigma$). Figure 3.3 presents an assessment of the diffraction of TE- and TM-waves on a dielectric cylinder.

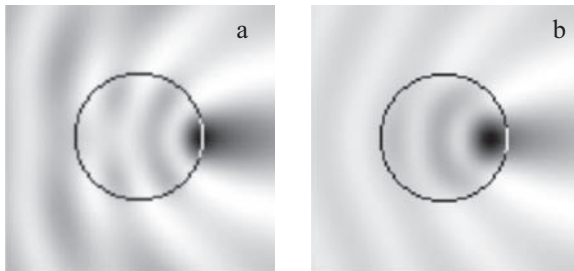


Fig. 3.1. Field intensity distribution of diffraction on a dielectric cylinder (inverted): TE polarization (a), TM polarization (b).

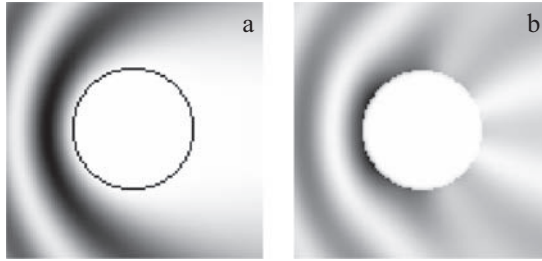


Fig. 3.2. Field intensity distribution of diffraction on a conducting cylinder (inverted): TE polarization (a), TM polarization (b).

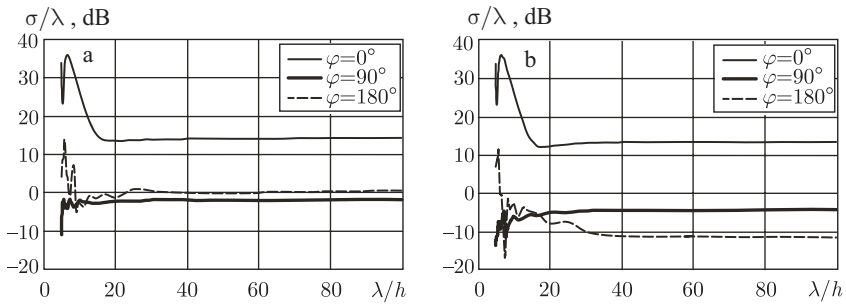


Fig. 3.3. The dependence of the directional diagram of scattering on a dielectric cylinder on parameter λ/h for the TE polarization (a) and TM polarization (b).

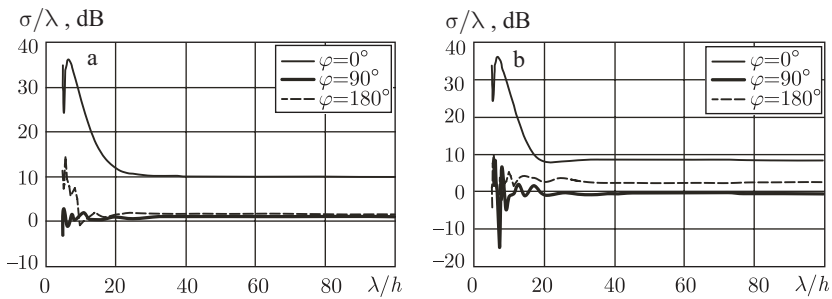


Fig. 3.4. The dependence of the directional diagram of scattering on a conducting cylinder on parameter λ/h for TE polarization (a) and TM polarization (b).

Figure 3.4 shows the dependence of the values of the directional diagram of diffraction of TE- and TM-waves on a conducting cylinder.

Figure 3.5 shows the dependence on the parameter λ/h of the values of the relative deviation of the directional diagram of scattering of TE- and TM-waves on a dielectric cylinder from the values at $\lambda/h = 100$ for the nodes φ equal to $0, \pi/2, \pi$.

Figure 3.6 shows the dependence on the parameter λ/h of the values of the relative deviation of the directional diagram of scattering of TE- and TM-waves on a conducting cylinder.

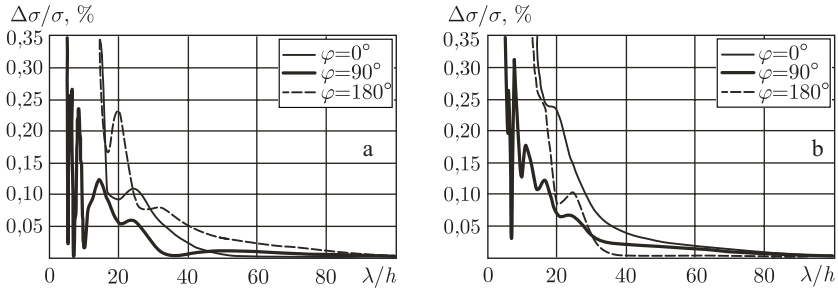


Fig. 3.5. Dependence of the relative deviation of the directional diagram of scattering on a dielectric cylinder on parameter λ/h for TE polarization (a) and TM polarization (b).

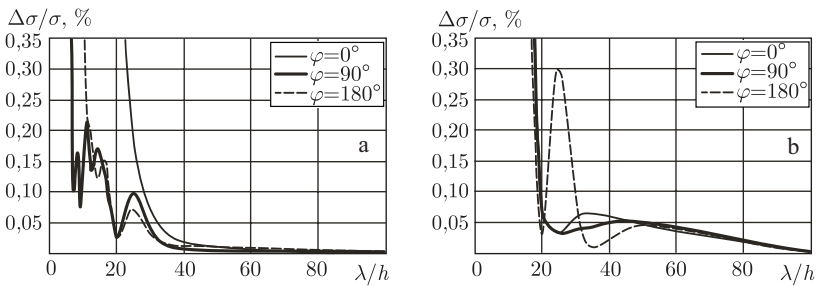


Fig. 3.6. Dependence of the relative deviation of the directional diagram of scattering on a conducting cylinder on parameter λ/h for TE polarization (a) and TM polarization (b).

A series of experiments with a dielectric cylinder showed that the relative deviation of the values of the directional diagram of scattering is less than 5% at $\lambda/h > 40$ and less than 1% at $\lambda/h > 80$ for both polarizations.

Experiments with the conducting cylinder showed that the relative deviation of the values of the directional diagram of scattering is less than 5% at $\lambda/h > 30$ for TE- polarization at $\lambda/h > 50$ for TM-polarization and less than 1% at $\lambda/h > 50$ for TE-polarization and at $\lambda/h > 80$ for TM-polarization.

Thus, the polarization state does not affect the results of modelling dielectric structures by the proposed method, but it must be taken into account when choosing the length of the segment of the coverage grid for the calculation of conductive structures with the corresponding relative error.

3.1.2. Analysis of the diffraction of light on periodic inhomogeneities

The theory of scattering on periodic structures, commonly referred to as diffraction gratings, has many applications in optics, such as electromagnetic and optical communications, visualization tools, determination of the properties of objects and surfaces, electronic and optical components, photonic crystals, diffraction gratings [32]. Numerical methods were developed to simulate the diffraction of light on

diffraction gratings. These methods include differential and integral methods, methods based on the propagation of Rayleigh and eigenmodes, the variational and finite-difference methods: the method of coupled waves (rigorous coupled wave analysis, RCWA) [33], C-method [34], finite element methods [35–37], the integral methods [21], finite difference-time domain (FDTD) methods [38, 39].

The variational methods are most effective for inhomogeneous problems with complex geometries. These methods require solving a linear system of equations with unloaded matrices. To reduce the size of the computational domain, the calculation of the field away from the computing domain can be performed using the integral relation. The material of a periodic structure can be dielectric, conducting, superconducting, the size of the inhomogeneities can be arbitrarily small. The corners of the profile of the geometry of the structure can be considered in calculations by the appropriate choice of the sampling grid.

As a special case of the variational methods we can consider the finite element method (FEM) applied to the elliptical Helmholtz equation in the calculation domain. It includes a choice of the discretization scheme, the construction and minimization of the functional relationships. The resulting ratio is converted to a system of linear equations which is incomplete without the use of boundary conditions.

For the boundary-value problem, satisfying the Sommerfeld radiation conditions, we can use methods of integral equations, respectively, the standard method of boundary elements can also be used for periodic tasks. Both methods are joined at the boundary between inner and outer parts, satisfying the conditions of continuity of the field. Using the finite element method to determine the field inside the object leads to a tridiagonal matrix which requires less computer memory and shorter computing time than the methods of the volume integrals. The result of using the boundary element method for determining the field at the boundary is a more accurate solution than using the finite element method with absorbing conditions of the boundary due to the strong dependence on the angle of incidence of the field on the boundary.

In this book, we describe the formulation of a combined method for problems of scattering of light by periodic objects based on the finite element method and the boundary element method (PFEM-BE). The developed PFEM-BE method and the RCWA method [40] were used for a comparative simulation of light diffraction on a dielectric one-dimensional diffraction grating. Comparison of the simulation results is presented for the TE- and TM-polarized waves.

Description of the calculation method

Consider the diffraction of a plane wave with wave vector $\mathbf{k} = k(\sin(\theta), -\cos(\theta), 0)$, $k = k_0\sqrt{\varepsilon}$ for the periodic structure with period d , k_0 is the wave number of the wave in free space $k_0 = 2\pi/\lambda_0$, where λ_0 is the wavelength in free space, ε is the dielectric constant of the medium.

The Light, diffracting on the structure, creates a scattered field. In addition to a decaying part, the diffracted light is split into a finite number of reflected and transmitted polarized plane waves whose propagation direction \mathbf{k} does not depend on

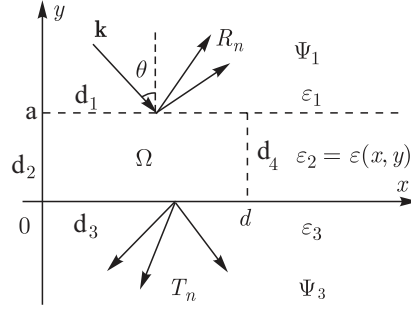


Fig. 3.7. Geometry of the diffraction problem on the periodic structure.

the geometry and material of the periodic structure, but depends only on the grating period. The total field is defined as the sum of the incident and scattered fields. The purpose of the task is to determine the amplitude and phase of reflected, transmitted and decaying orders.

The geometry of the problem is shown in Fig. 3.7, where R_n and T_n are the reflection and transmission coefficients of the diffraction orders. For the given geometry of the problem we define three zones with different dielectric constants: the area above the structure at $y > a$ (Ψ_1), where a is the maximum height of the structure, with a dielectric permittivity constant $\varepsilon = \varepsilon_1$, the region of the structure $0 < y < a$ with dielectric permittivity $\varepsilon = \varepsilon(x, y)$, and the $y < 0$ (Ψ_3) with a constant dielectric permittivity $\varepsilon = \varepsilon_3$.

The diffraction of a plane wave on a one-dimensional periodic structure is reduced to two independent problems: the problem of diffraction of a plane wave with TE-polarization ($E_z \neq 0, H_z = 0$) and the problem of diffraction of a plane wave with TM-polarization ($H_z \neq 0, E_z = 0$) [41].

The total field $u_\Omega(x, y)$ in the region Ω ($0 < x < d, 0 < y < a$) must satisfy the following equation [42]:

$$\nabla \cdot \left[\frac{1}{p(x, y)} \nabla u_\Omega(x, y) \right] + k_0^2 q(x, y) u_\Omega(x, y) = f_\Omega, \quad (3.29)$$

where $f_\Omega = jk_0 Z_0 J_z, p(x, y) = \mu_r, q(x, y) = \varepsilon_r$ for TE-polarization, and $f_\Omega = - \left[\nabla \times \left(\frac{\mathbf{J}^\Omega}{\varepsilon_\Omega} \right) \right] \cdot \mathbf{z}$,

$p(x, y) = \varepsilon_r$ for TM-polarization. Constants μ_r and ε_r are the ratio of magnetic and dielectric constants of the medium to the same parameters of free space, i.e. $\mu_r = \mu / \mu_0$ and $\varepsilon_r = \varepsilon / \varepsilon_0$, $Z_0 = \sqrt{\mu_0 / \varepsilon_0}$ is the impedance of free space, $\mathbf{J}^\Omega = (J_x, J_y, J_z)$ is the vector of the electric current density of the source in region Ω . For TE-polarization, the complex amplitude $u(x, y)$ denotes the total electric field $E_z(x, y)$, which is directed along the axis z (along the generatrix of a cylindrical optical element), the coordinates (x, y) lie in the plane of the normal section. For TM-polarization the complex amplitude $u(x, y)$ denotes the total magnetic field $H_z(x, y)$.

To solve (3.29), the computing domain Ω should be limited by the introduction of the artificial boundary $\Gamma = \Gamma_1 + \Gamma_2 + \Gamma_3 + \Gamma_4$ (see Fig. 3.7). Γ_1 and Γ_3 are the

fictitious boundaries, infinitely extending parallel to the x -axis of the coordinates $y = a$ and $y = 0$. Accordingly, for the unique solution of the problem boundary conditions must be imposed at the given artificial boundary.

Since the space in zones Ψ_1 and Ψ_3 is homogeneous, the field in these zone can be defined in terms of boundary integrals with the appropriate Green's function. The total field $u_\Psi(x, y)$ in these zones must satisfy the following equation:

$$\nabla \cdot \left[\frac{1}{p} \nabla u_\Psi(\xi) \right] + k_0^2 q u_\Psi(\xi) = f_\Psi, \quad \xi \in \Psi, \quad (3.30)$$

CORRECT THIS

where $f_\Psi = jk_0 Z_0 J_z^\Psi$, $p = \mu_\Psi$, $q = \varepsilon_\Psi$ for TE-polarization,

$$f_\Psi = - \left[\nabla \times \left(\frac{J^\Psi}{\varepsilon_\Psi} \right) \right] \cdot \mathbf{z}, \quad p = \varepsilon_\Psi, \quad q = \mu_\Psi$$

for TM-polarization. J_Ψ is the vector of electric current density of the source in the region Ψ , the region $\Psi = \Psi_1, \Psi_3$.

Application of the Galerkin method to the solution of (3.30) in the region Ψ of the periodic structure is similar to the approach described in §3.1.1, to obtain the system of equations (3.15).

We define the boundary conditions for the field and its derivatives at the boundaries of Γ_1 and Γ_3 to complement the system (3.15). To construct the boundary integral equation for the field and its normal derivative, we introduce the Green function u^* which satisfies the Sommerfeld radiation conditions and is the fundamental solution of the Helmholtz equation in semi-infinite domains Ψ_1 and Ψ_3 :

$$\nabla^2 u^*(\xi, \eta) + k^2 u^*(\xi, \eta) = -\delta(\xi, \eta), \quad \xi, \eta \in \Psi_1, \Psi_3. \quad (3.31)$$

The fundamental solution for the Helmholtz equation in two-dimensional homogeneous space is well known and well

$$u^*(\xi, \eta) = (i/4) H_0^{(1)}(kr), \quad (3.32)$$

where $r = \sqrt{[x(\eta) - x(\xi)]^2 + [y(\eta) - y(\xi)]^2}$, $H_0^{(1)}(kr) = J_0(kr) + iY_0(kr)$ is the Hankel function of the first kind and zero order, where J_0 is the Bessel function of zero order, Y_0 is the Neumann function of zero order.

To construct the boundary integral equation for the scattered field and its normal derivative in zones Ψ_1 and Ψ_3 , we use Green's theorem as follows:

$$h(\theta) = \delta(\theta), \quad (3.33)$$

where $v(\eta) = \partial u(\eta) / \mathbf{n}'$ are the normal derivatives of the field, and Γ' represents the infinite boundaries $y = a$ and $y = 0$ for zones Ψ_1 and Ψ_3 , respectively.

Substituting (3.31) into equation (3.33), passing to the limit of the observation point ξ from the inner to the boundary ??? and using (3.21), we obtain

$$\frac{1}{2}u(\xi) = -\int_{\Psi} f_{\Psi}(\eta)u^*(\xi, \eta)d\Psi + \int_{\Gamma'} \nu(\eta)u^*(\xi, \eta)d\Gamma - \int_{\Gamma'} u(\eta)\frac{\partial u^*(\xi, \eta)}{\partial \mathbf{n}'}d\Gamma, \quad \Psi = \Psi_1, \Psi_3. \quad (3.34)$$

This equation provides a functional link between the functions u and its normal derivative ν on the boundary Γ' . The first term on the right side of (3.34) is the field produced by the source f_{Ψ} in free space, and may be designated as the incident field u_{Ψ}^{in} .

Thus, equation (3.34) is written as follows:

$$\frac{1}{2}u(\xi) = \int_{\Gamma'} \nu(\eta)u^*(\xi, \eta)d\Gamma - \int_{\Gamma'} u(\eta)\frac{\partial u^*(\xi, \eta)}{\partial \mathbf{n}'}d\Gamma + u_{\Psi}^{\text{in}}(\xi). \quad (3.35)$$

Field u and its derivatives ν in the case of the diffractive grating are quasi-periodic functions [41, 43–45]:

$$\begin{aligned} u(x, y) &= \tilde{u}(x, y)e^{ik_0\alpha_0x}, \\ \nu(x, y) &= \tilde{\nu}(x, y)e^{ik_0\alpha_0x}, \end{aligned} \quad (3.36)$$

where $\tilde{u}(x, y)$ and $\tilde{\nu}(x, y)$ are periodic functions with respect to x with period d .

The integration over the infinite boundary Γ' in (3.35) can be replaced by integration along the boundaries Γ_1 and Γ_3 :

$$\begin{aligned} \frac{1}{2}u(x_0, y) &= \int_{\Gamma} \sum_{n=-\infty}^{\infty} \tilde{\nu}(x, y)e^{ik_0\alpha_0(x+nd)}u^*(x+nd-x_0)dx - \\ &- \int_{\Gamma} \sum_{n=-\infty}^{\infty} \tilde{u}(x, y)e^{ik_0\alpha_0(x+nd)}\frac{\partial u^*(x+nd-x_0)}{\partial \mathbf{n}'}dx + u^{\text{in}}(x_0, y), \quad x \in [0, d), \end{aligned} \quad (3.37)$$

where $\Gamma = \Gamma_1$, $\Gamma_1, y = a$ and $y = 0$ on boundaries Γ_1 and Γ_3 , respectively.

Substituting the function of the complex amplitude in equation (3.37) on the boundary of its basic approximation of piecewise linear functions (3.8) and (3.9), we obtain:

$$\begin{aligned} \frac{1}{2}u_{\Gamma_i}(x_s) &= \sum_{m=1}^M h \left\{ \nu_{\Gamma_i}(x_m) \sum_{n=-\infty}^{\infty} e^{ik_0\alpha_0(x_m+nd)} \left[\int_{-1}^1 \omega^{\Gamma_i}(x_m+h\eta)u_{\Gamma_i}^*(x_m+nd-x_s+h\eta)d\eta \right] - \right. \\ &\left. - u_{\Gamma_i}(x_m) \sum_{n=-\infty}^{\infty} e^{ik_0\alpha_0(x_m+nd)} \left[\int_{-1}^1 \omega^{\Gamma_i}(x_m+h\eta)\frac{\partial u_{\Gamma_i}^*(x_m+nd-x_s+h\eta)}{\partial \mathbf{n}'}d\eta \right] \right\} + u_{\Gamma_i}^{\text{in}}(x_s), \end{aligned} \quad (3.38)$$

where $s = [1, N_{x-1}]$, $i = 1, 3$.

The boundary conditions on the field and its derivatives at the boundaries Γ_2 and Γ_4 are periodic of the form:

$$u_{\Gamma_4} = u_{\Gamma_2} e^{ik_0\alpha_0 d}, \quad v_{\Gamma_4} = v_{\Gamma_2} e^{ik_0\alpha_0 d}. \quad (3.39)$$

The expansions (3.8) and (3.9) and boundary conditions (3.39) can be written for the coefficients of the field and its derivatives at the boundaries Γ_2 and Γ_4 :

$$u_{\Gamma_4}(x_s) = u_{\Gamma_2}(x_s) e^{ik_0\alpha_0 d}, \quad v_{\Gamma_4}(x_s) = v_{\Gamma_2}(x_s) e^{ik_0\alpha_0 d}, \quad (3.40)$$

where $s = [1, N_y]$. Elements of the matrices \mathbf{D} and \mathbf{G} , corresponding to the boundaries Γ_2 and Γ_4 , can be written as:

$$d_2^s = 1, \quad d_4^s = d_2^s e^{ik_0\alpha_0 d}, \quad g_2^s = 1, \quad g_4^s = g_2^s e^{ik_0\alpha_0 d}, \quad e_2^s = 0, \quad e_4^s = 0, \quad s = [1, N_y]. \quad (3.41)$$

Elements of the matrices \mathbf{D} and \mathbf{G} , corresponding to the boundaries Γ_1 and Γ_3 , can be written as:

$$d_i^{s,m} = -h \left\{ \sum_{n=-\infty}^{\infty} e^{ik_0\alpha_0(x_m+nd)} \left[\int_{-1}^1 \omega^{\Gamma_i}(x_m+h\eta) \frac{\partial u_{\Gamma_i}^*(x_m+nd-x_s+h\eta)}{\partial \mathbf{n}'} d\eta \right] \right\}, \quad e_i^s = \frac{1}{2} \delta_{s,m}, \quad (3.42)$$

$$g_i^{s,m} = h \left\{ \sum_{n=-\infty}^{\infty} e^{ik_0\alpha_0(x_m+nd)} \left[\int_{-1}^1 \omega^{\Gamma_i}(x_m+h\eta) u_{\Gamma_i}^*(x_m+nd-x_s+h\eta) d\eta \right] \right\}, \quad (3.43)$$

$$k\sqrt{\varepsilon_i} \tau_i, \quad m, s = [1, N_{x-1}], \quad i = 1, 3.$$

The relations (3.38) can be represented in matrix form:

$$[\mathbf{D}]\mathbf{u}_{\Gamma} + [\mathbf{G}]\mathbf{v}_{\Gamma} = [\mathbf{E}]u_{\Gamma}^{in} \quad (3.44)$$

with elements of the matrices \mathbf{D} , \mathbf{G} and \mathbf{E} of the form (3.41) (3.42) and (3.43). Infinite series in (3.42) and (3.43) are approximated by finite sums, integrals can be evaluated numerically. Combining equations (3.15) and (3.44), we obtain a closed system of linear algebraic equations for solving the problem of diffraction of a plane wave on a periodic two-dimensional micro-object:

$$\begin{bmatrix} [\mathbf{A}_{\Omega,\Omega}] & [\mathbf{A}_{\Gamma,\Omega}] & \mathbf{0} \\ [\mathbf{A}_{\Omega,\Gamma}] & [\mathbf{A}_{\Gamma,\Gamma}] & [\mathbf{B}] \\ \mathbf{0} & [\mathbf{D}] & [\mathbf{G}] \end{bmatrix} \begin{bmatrix} \mathbf{u}_{\Omega} \\ \mathbf{u}_{\Gamma} \\ \mathbf{v}_{\Gamma} \end{bmatrix} = \begin{bmatrix} [\mathbf{C}_{\Omega,\Omega}] & [\mathbf{C}_{\Gamma,\Omega}] & \mathbf{0} \\ [\mathbf{C}_{\Omega,\Gamma}] & [\mathbf{C}_{\Gamma,\Gamma}] & \mathbf{0} \\ \mathbf{0} & \mathbf{0} & [\mathbf{E}] \end{bmatrix} \begin{bmatrix} \mathbf{f}_{\Omega} \\ \mathbf{f}_{\Gamma} \\ \mathbf{u}_{\Gamma}^{in} \end{bmatrix}, \quad (3.45)$$

where the submatrix $\mathbf{A}_{\Omega,\Omega}$ with the dimension $(N-M) \times (N-M)$ includes the ratio of the field in the internal nodes of the partition grid, submatrices $\mathbf{A}_{\Omega,\Gamma}$ and $\mathbf{A}_{\Gamma,\Omega}$ with the dimension $(N-M) \times M$ and $M \times (N-M)$, respectively, include the

coupling coefficients of the field at the boundary nodes, the \mathbf{A}_{Γ} submatrix with the size $M \times M$ involves the coupling coefficients of the field at the boundary nodes, the submatrix \mathbf{B} with the size $M \times M$ includes the ratio between the derivatives of the field at the boundary and the field in the internal nodes of the partition grid, submatrix \mathbf{D} with the size $M \times M$ involves the coupling coefficients of the field of free space at the boundary nodes, the submatrix \mathbf{G} with the size $M \times M$ includes the ratio between the derivatives of the field at the boundary and the field of free space in the internal nodes of the partition grid. Submatrix $\mathbf{C}_{\Omega, \Omega}$ with the dimension $(N - M) \times (N - M)$ includes the ratio of field sources in the internal nodes of the partition, submatrix $\mathbf{C}_{\Omega, \Gamma}$ and $\mathbf{C}_{\Gamma, \Omega}$ with the dimension $(N - M) \times M$ and $M \times (N - M)$, respectively, include the ratio of field sources in the boundary and internal nodes, the submatrix $\mathbf{C}_{\Gamma, \Gamma}$ with the size of $M \times M$ includes the ratio of the field sources at the boundary nodes. Submatrix \mathbf{E} has size $M \times M$. Vector \mathbf{u}_{Ω} and \mathbf{u}_{Γ} are the field vectors in the interior and boundary nodes, \mathbf{v}_{Γ} is the vector of normal derivatives of the field at the boundary nodes of the grid. Vectors \mathbf{f}_{Ω} and \mathbf{f}_{Γ} are the vectors of the field sources in the interior and boundary nodes of the grid, $\mathbf{u}_{\Gamma}^{\text{in}}$ is the vector of the external incident field at the boundary nodes of the grid. Thus, the system (3.45) has $N + M$ equations and the same number of unknowns.

The field in the areas of Ψ_1 and Ψ_3 can be represented by a Rayleigh expansion (superposition of plane waves). In the area Ψ_1 the z -components of the fields are as follows:

$$u(x, y) = \exp(ik_0(\alpha_0 x - \beta_0 y)) + \sum_{n=-\infty}^{\infty} R_n \exp(ik_0(\alpha_n x + \beta_n y)), \quad (3.46)$$

where

$$\alpha_n = \sqrt{\varepsilon_1} \sin(\theta) + n \frac{\lambda_0}{d}, \quad \beta_n = \sqrt{\varepsilon_1 - \alpha_n^2}. \quad (3.47)$$

The function $u(x, y)$ is the component $E_z(x, y)$ of the electric field for the case of TE-polarization and the component $H_z(x, y)$ of the magnetic field for TM-polarization.

In zone Ψ_3 the z -component are as follows:

$$u(x, y) = \sum_{n=-\infty}^{\infty} T_n \exp(ik_0(\alpha_n x - \tilde{\beta}_n y)), \quad (3.48)$$

where

$$\tilde{\beta}_n = \sqrt{\varepsilon_3 - \alpha_n^2}. \quad (3.49)$$

Rayleigh expansions (3.46) and (3.48) are solutions of the Helmholtz equation,

$$k^2 = k_0^2 \varepsilon_3 \quad (3.50)$$

at $k^2 = k_0^2 \varepsilon_1$ and $k^2 = k_0^2 \varepsilon_3$ respectively.

After determining the values of the field in the region Ω and its derivatives at the boundaries Γ_1 and Γ_3 the normalized intensities of the reflected and transmitted orders are calculated as follows [32, 36, 37]:

$$I_n^R = |R_n|^2 \frac{\beta_n}{\beta_0}, \quad I_n^T = \sqrt{\frac{\varepsilon_3}{\varepsilon_1}} |T_n|^2 \frac{\tilde{\beta}_n}{\beta_0}, \quad \left(\sum_{n \in U_1} I_n^R + \sum_{n \in U_3} I_n^T = 1 \right), \quad (3.51)$$

$$I_n^R = |R_n|^2 \frac{\beta_n}{\beta_0}, \quad I_n^T = \sqrt{\frac{\varepsilon_1}{\varepsilon_3}} |T_n|^2 \frac{\tilde{\beta}_n}{\beta_0}, \quad \left(\sum_{n \in U_1} I_n^R + \sum_{n \in U_3} I_n^T = 1 \right) \quad (3.52)$$

for TE- and TM-polarized waves, respectively. Expressions (3.36) and (3.37) determine what portion of the energy of the incident wave will move to the n -th order of diffraction. Note that the intensities of the propagation distribution are for non-absorbing materials, i.e. for $\text{Im}\sqrt{\varepsilon_i} = 0$. The sets U_1 and U_2 in (3.51) and (3.52) are the sets of indices corresponding to the reflected and transmitted diffraction orders:

$$U_1 = \begin{cases} \left\{ n \in Z : \frac{\alpha_n^2}{\varepsilon_1} < 1 \right\}, & \text{Im}\sqrt{\varepsilon_1} = 0 \\ 0, & \text{Im}\sqrt{\varepsilon_1} > 0 \end{cases}, \quad U_3 = \begin{cases} \left\{ n \in Z : \frac{\alpha_n^2}{\varepsilon_3} < 1 \right\}, & \text{Im}\sqrt{\varepsilon_3} = 0 \\ 0, & \text{Im}\sqrt{\varepsilon_3} > 0 \end{cases}. \quad (3.53)$$

To determine the coefficients of reflection R_n and transmission T_n , we use the discrete Fourier transform:

$$R_n = \frac{1}{N} \sum_{k=0}^{N-1} \left[u(x_k, a) - u^{in}(x_k, a) \right] \exp(-ik_0 \alpha_n x_k). \quad (3.54)$$

$$T_n = \frac{1}{N} \sum_{k=0}^{N-1} u(x_k, 0) \exp(-ik_0 \alpha_n x_k). \quad (3.55)$$

These coefficients describe the amplitude and phase shift of propagating plane waves. More precisely, the modules $|R_n|$ and $|T_n|$ are the amplitudes of the n -th reflected and transmitted orders and $\arg [R_n/R_n]$ and $\arg [T_n/T_n]$ are the phase shifts. The coefficients with $n \in U_1$, $n \in U_3$ describe the damped waves.

Examples of calculation

For example, consider the diffraction of a plane wave with wavelength $\lambda_0 = 0.6 \mu\text{m}$ on a binary dielectric diffraction grating with a fill factor of 0.25 and with a thickness of $0.24 \mu\text{m}$. The grating period was varied from $0.2 \mu\text{m}$ to $2 \mu\text{m}$. Accordingly, in

simulation by PFEM-BE the length of the segment of the coating grid varied from $\lambda_0/300$ to $\lambda_0/30$.

Consider an example. A plane wave is incident along the normal from the air ($\epsilon_1 = 1$) on the grating ($\epsilon_3 = 2.25$). Figures 3.8 and 3.9 show the dependence of the efficiencies I_0^R and I_0^T orders of diffraction of TE- and TM-polarized waves, respectively, on the grating period.

Dependences of deviations of intensities ΔI_0^R and ΔI_0^T ($\Delta I = |I_i^{RCWA} - I_i^{PFEM-BE}|$) of zero-order diffraction, calculated by RCWA and PFEM-BE methods, of the TE- and TM-polarized waves on the length of the segment of the coating grid h in the PFEM-BE method, are shown in Fig. 3.10. It is difficult to note the explicit dependence of the deviation for $h < \lambda_0/30$. The uniform rate of deviation of the intensities is $4 \cdot 10^{-3}$ and $2 \cdot 10^{-3}$ for the TE- and TM-polarizations, respectively.

In the following example, a plane wave is incident along the normal from the substrate of the grating ($\epsilon_3 = 2.25$) in air ($\epsilon_3 = 1$). Figures 3.11 and 3.12 show the dependence of the intensities I_0^R and I_0^T of the diffraction orders of TE- and TM-polarized waves on the grating period.

Depending on the deviations of the intensities ΔI_0^R and orders I_0^T of diffraction orders of TE- and TM-polarized waves, the length of the segment of

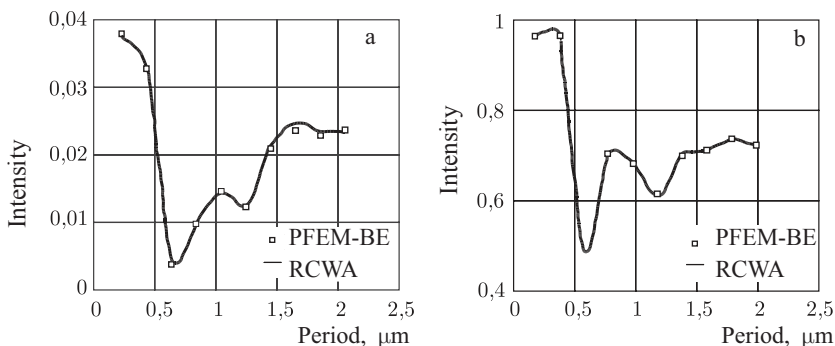


Fig. 3.8. Distribution of the effectiveness of zero-order diffraction of TE-polarized wave: a) I_0^R ; b) I_0^T .

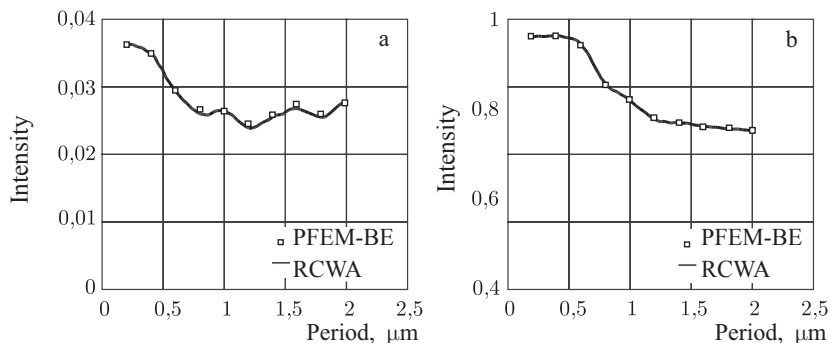


Fig. 3.9. Distribution of the effectiveness of zero order diffraction of TM-polarized wave: a) I_0^R ; b) I_0^T .

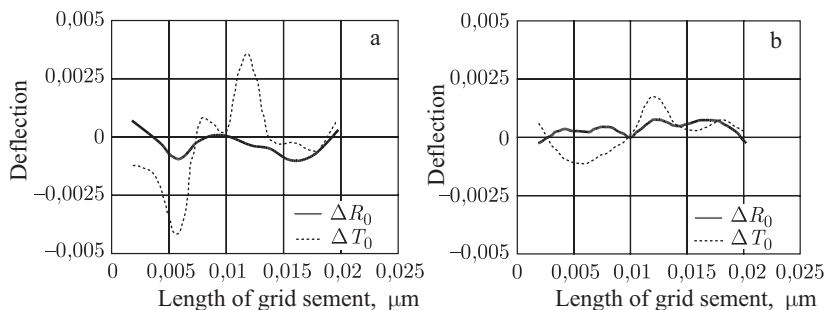


Fig. 3.10. The dependence of the deviations of the efficiency of zero orders on parameter h : a) TE-waves and b) TM waves.

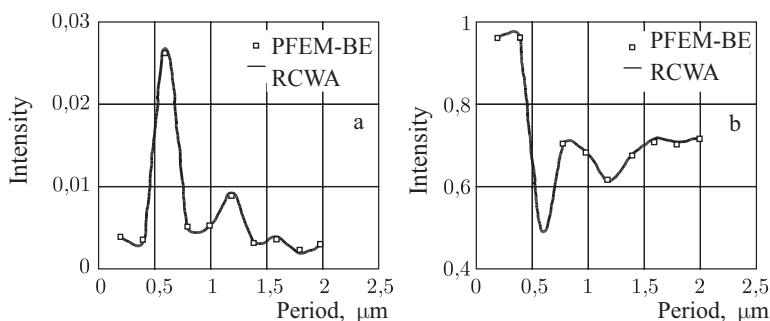


Fig. 3.11. Distribution of the effectiveness of zero-order diffraction of TE-polarized waves: a) I_0^R ; b) I_0^T .

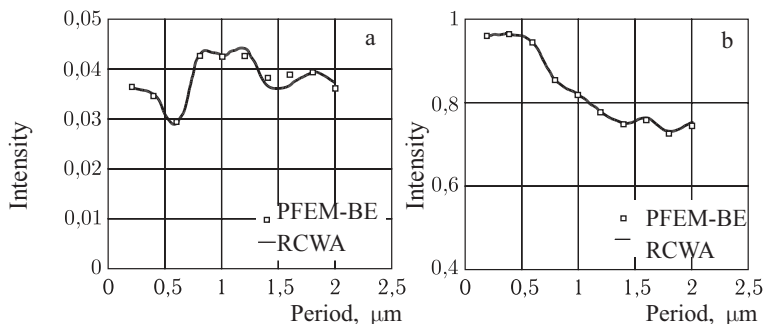


Fig. 3.12. Distribution of the effectiveness of zero-order diffraction of TM-polarized waves: a) I_0^R ; b) I_0^T .

the coating h are shown in Fig. 3.13. The uniform rate of deviation of the intensities is $7 \cdot 10^{-3}$ and $8 \cdot 10^{-3}$ for the TE- and TM-polarizations, respectively.

Thus, the comparison of results obtained by the PFEM-BE and RCWA methods shows that they are in good agreement.

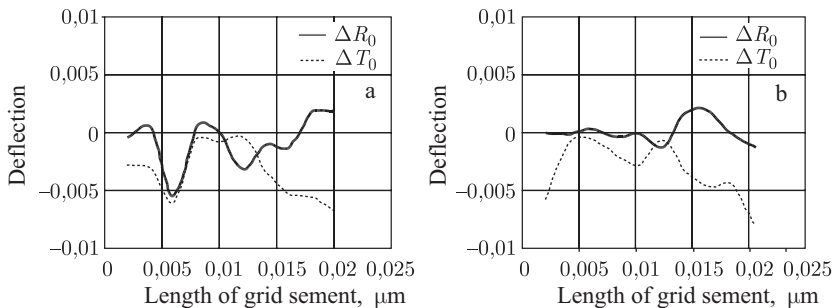


Fig. 3.13. Dependence of the deviations of the efficiency of zero orders on parameter h ; a)

3.2. Finite element methods for solving the two-dimensional integral diffraction equation

3.2.1. TE-polarization

In [1, 30, 42] the scalar problem of diffraction on a transparent body with an inhomogeneous refractive index is reduced to the Fredholm integral equation of the second kind. This chapter discusses the 2D vector diffraction problem for objects with the uneven and, in general, complex refractive index. The resulting integral equation for the cases of TE- and TM-polarization of the incident electromagnetic wave is solved by the finite element method (FEM) [46].

We define the geometry of the problem, as shown in Fig. 3.14.

A cylindrical object has infinite length along the axis z , and its cross-section lies in the plane (x, y) . The plane of incidence of the wave coincides with the plane (x, y) .

Figure 3.14 gives the following notation: Ω_1 – area of the transparent body bounded by contour S with the function of the dielectric permittivity $\epsilon_1(x, y)$, magnetic permeability $k_2 = 2\pi / \lambda \sqrt{\epsilon_2 \mu_2}$, Ω_2 – the outside homogeneous region with constant properties ϵ_2 and μ_2 . Furthermore, we assume that $\mu_1 = \mu_2 = 1$.

From Maxwell's equations [47]:

$$\text{rot } \mathbf{E} + \frac{1}{c} \dot{\mathbf{B}} = 0 \tag{3.56}$$

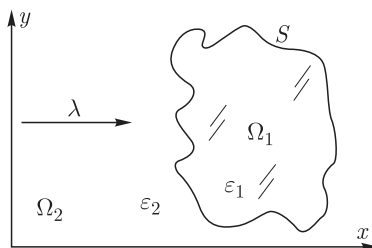


Fig. 3.14. Diffraction of an electromagnetic wave on an inhomogeneous transparent body.

and the material equation for an isotropic medium

$$\mathbf{B} = \mu \mathbf{H} \quad (3.57)$$

given the fact that

$$\text{rot } \mathbf{E} = \mathbf{i} \left(\frac{\partial E_z}{\partial y} - \frac{\partial E_y}{\partial z} \right) + \mathbf{j} \left(\frac{\partial E_x}{\partial z} - \frac{\partial E_z}{\partial x} \right) + \mathbf{k} \left(\frac{\partial E_y}{\partial x} - \frac{\partial E_x}{\partial y} \right),$$

$$\dot{\mathbf{B}} = \mu \dot{\mathbf{H}} = \mu \left(\mathbf{i} \frac{\partial H_x}{\partial t} + \mathbf{j} \frac{\partial H_y}{\partial t} + \mathbf{k} \frac{\partial H_z}{\partial t} \right),$$

we get

$$\begin{aligned} \frac{\partial E_z}{\partial y} - \frac{\partial E_y}{\partial z} + \frac{1}{c} \mu \frac{\partial H_x}{\partial t} &= 0, \\ \frac{\partial E_x}{\partial z} - \frac{\partial E_z}{\partial x} + \frac{1}{c} \mu \frac{\partial H_y}{\partial t} &= 0, \\ \frac{\partial E_y}{\partial x} - \frac{\partial E_x}{\partial y} + \frac{1}{c} \mu \frac{\partial H_z}{\partial t} &= 0. \end{aligned} \quad (3.58)$$

For monochromatic radiation ($E e^{-i\omega t}$), system (3.58) takes the form:

$$\begin{aligned} \frac{\partial E_z}{\partial y} - \frac{\partial E_y}{\partial z} - \frac{i\omega}{c} \mu H_x &= 0, \\ \frac{\partial E_x}{\partial z} - \frac{\partial E_z}{\partial x} - \frac{i\omega}{c} \mu H_y &= 0, \\ \frac{\partial E_y}{\partial x} - \frac{\partial E_x}{\partial y} - \frac{i\omega}{c} \mu H_z &= 0. \end{aligned} \quad (3.59)$$

Here ω is the angular frequency of oscillations. We denote $k_0 = \omega/c = 2\pi/\lambda$, where λ is the wavelength of light. In the case of 2D problems, system (3.59) takes the form:

$$\frac{\partial E_z}{\partial y} - ik_0 \mu H_x = 0, \quad (3.60)$$

$$-\frac{\partial E_z}{\partial x} - ik_0 \mu H_y = 0, \quad (3.61)$$

$$\frac{\partial E_y}{\partial x} - \frac{\partial E_x}{\partial y} - ik_0 \mu H_z = 0. \quad (3.62)$$

According to the above reasoning of Maxwell's equations

$$\operatorname{rot} \mathbf{H} - \frac{1}{c} \dot{\mathbf{D}} = \frac{4\pi}{c} \mathbf{j} \quad (3.63)$$

and constitutive equation

$$\mathbf{D} = \varepsilon \mathbf{E} \quad (3.64)$$

in the absence of external currents, we obtain

$$\frac{\partial H_z}{\partial y} + ik_0 \varepsilon E_x = 0, \quad (3.65)$$

$$-\frac{\partial H_z}{\partial x} + ik_0 \varepsilon E_y = 0, \quad (3.66)$$

$$\frac{\partial H_y}{\partial x} - \frac{\partial H_x}{\partial y} + ik_0 \varepsilon E_z = 0. \quad (3.67)$$

Using equations (3.60), (3.61) and (3.67), we get a scalar Helmholtz equation

$$\frac{\partial}{\partial x} \left(\frac{\partial E_z}{\partial x} \right) + \frac{\partial}{\partial y} \left(\frac{\partial E_z}{\partial y} \right) + k_0^2 \varepsilon \mu E_z = 0. \quad (3.68)$$

We denote the field E_z in Ω_1 by E_z^{in} , and in Ω_2 by E_z^{ext} . Then the problem of diffraction on the object Ω_1 is reduced to solving the system of differential Helmholtz equations [30]:

$$\left(\Delta + k_1^2(x, y) \right) E_z^{\text{in}} = 0, \quad (x, y) \in \Omega_1, \quad (3.69)$$

$$\left(\Delta + k_2^2 \right) E_z^{\text{ext}} = -g_2, \quad (x, y) \in \Omega_2, \quad (3.70)$$

where g_2 is the function describing the source in the external field Ω_2 , $k_1(x, y) = k_0 \sqrt{\varepsilon_1(x, y) \mu}$ is the wave number for the field Ω_2 with an inhomogeneous refractive index, $k_2 = k_0 \sqrt{\varepsilon_2 \mu_2}$ is the wave number for Ω_2 . Here $\Delta = \frac{\partial^2}{\partial x^2} + \frac{\partial^2}{\partial y^2}$

For TE-polarization, the boundary conditions (BC) follow from the continuity at the interface between two media of the tangential components of electric and magnetic fields [47]:

$$\begin{aligned} [\mathbf{n}_1, \mathbf{E}_1] - [\mathbf{n}_1, \mathbf{E}_2] &= 0, \\ [\mathbf{n}_1, \mathbf{H}_1] - [\mathbf{n}_1, \mathbf{H}_2] &= \mathbf{j}_{\text{surf}}. \end{aligned} \quad (3.71)$$

Here $\mathbf{j}_{\text{surf}} = 0$, \mathbf{n}_1 is the vector the outward normal to the field Ω_1 .

Equations (3.71) give the BCs SU for the fields E_z^{in} and E_z^{ext} .

$$E_z^{in} \Big|_S = E_z^{ext} \Big|_S, (x, y) \in S, \quad (3.72)$$

$$\frac{\partial E_z^{in}}{\partial \mathbf{n}_1} \Big|_S = -\frac{\partial E_z^{ext}}{\partial \mathbf{n}_2} \Big|_S, (x, y) \in S. \quad (3.73)$$

Here \mathbf{n}_2 is the vector of the normal (external to the region Ω_2) to the contour S .

The external field E_z^{ext} satisfies the Sommerfeld radiation condition:

$$\frac{\partial E_z^{ext}}{\partial r} - ik_2 E_z^{ext} = o\left(\frac{1}{r}\right) \text{ at } r \rightarrow \infty \quad (3.74)$$

For function E_z^{in} and Green's functions G_2 in the region Ω_2 we have the scalar Green's formula [48]:

$$\iint_{\Omega_1} (E_z^{in} \Delta G_2 - G_2 \Delta E_z^{in}) dx dy = \oint_S \left(E_z^{in} \frac{\partial G_2}{\partial \mathbf{n}_1} - G_2 \frac{\partial E_z^{in}}{\partial \mathbf{n}_1} \right) dS. \quad (3.75)$$

From equations (3.69) and (3.70) it follows

$$\begin{aligned} \Delta E_z^{in} &= -k_1^2(x, y) E_z^{in}, \\ \Delta E_z^{ext} &= -k_2^2 E_z^{ext} - g_2. \end{aligned} \quad (3.76)$$

The following equality holds for function G_2

$$\Delta G_2 + k_2^2 G_2 = -\delta(M, M_0), \quad (3.77)$$

where M is the current point at which the integration is carried out, M_0 is the point of observation, i.e. $\delta(M, M_0) = \delta(x', y'; x, y) - \delta$ -function.

Substituting equations (3.76) and (3.77) into equation (3.75), we obtain

$$\begin{aligned} \oint_S \left(G_2 \frac{\partial E_z^{in}}{\partial \mathbf{n}_1} - E_z^{in} \frac{\partial G_2}{\partial \mathbf{n}_1} \right) dS + \iint_{\Omega_1} (k_1^2 - k_2^2) E_z^{in} G_2 dx dy \\ - \iint_{\Omega_1} E_z^{in}(x', y') \delta(x', y'; x, y) dx' dy' = 0. \end{aligned} \quad (3.78)$$

Using the filtering properties of the δ -function, we reduce equation (3.78) to the form

$$\oint_S \left(G_2 \frac{\partial E_z^{in}}{\partial \mathbf{n}_1} - E_z^{in} \frac{\partial G_2}{\partial \mathbf{n}_1} \right) dS + \iint_{\Omega_1} (k_1^2 - k_2^2) E_z^{in} G_2 dx dy = \begin{cases} E_z^{in}, & (x, y) \in \Omega_1 \\ 0, & (x, y) \in \Omega_2 \end{cases}. \quad (3.79)$$

Similarly, applying Green's formula for functions E_z^{ext} and G_2 by using equations (3.76) and (3.77), we obtain

$$\oint_S \left(G_2 \frac{\partial E_z^{\text{ext}}}{\partial \mathbf{n}_2} - E_z^{\text{ext}} \frac{\partial G_2}{\partial \mathbf{n}_2} \right) dl + \iint_{\Omega_2} g_2 G_2 dx dy = \begin{cases} 0, & (x, y) \in \Omega_1 \\ E_z^{\text{ext}}, & (x, y) \in \Omega_2 \end{cases}. \quad (3.80)$$

Adding the equations (3.79) and (3.80) with the boundary conditions (3.72) and (3.73), we obtain

$$\iint_{\Omega_1} (k_1^2 - k_2^2) E_z^{\text{in}} G_2 dx dy + E_{0z} = \begin{cases} E_z^{\text{in}}, & (x, y) \in \Omega_1 \\ E_z^{\text{ext}}, & (x, y) \in \Omega_2 \end{cases}, \quad (3.81)$$

where

$$E_{0z}(x, y) = \iint_{\Omega_2} g_2 G_2 dx dy$$

is the field in the region Ω_1 or Ω_2 created by the sources with the function $g_2(x, y)$. According to the condition of the problem, the field E_0 is known.

If $(x, y) \in \Omega_1$, the first of equations (3.79) is a Fredholm integral equation of second kind with respect to E_z^{in} and at $E_{0z} \neq 0$ has a unique non-trivial solution [30].

Further assume that the point source is far away from the region Ω_1 and $E_{0z}(x, y)$ can be regarded as a plane wave. Consider the case where a plane wave is incident along the x axis from left to right in the chosen coordinate system (Fig. 3.14):

$$E_{0z} = \exp(ik_2 x). \quad (3.82)$$

The Green's function in region Ω_2 for 2D optical fields, satisfying the radiation condition, is [49]:

$$G_2(\xi) = \frac{i}{4} H_0^{(1)}(\xi), \quad (3.83)$$

where $\xi = k_2 \sqrt{(x-x')^2 + (y-y')^2}$, $H_0^{(1)}(\xi)$ is the Hankel function of first kind of zero order [50].

The field E_z , located in the system (3.81), is substituted into equation (3.60) (3.61), from which the components H_x , H_y of the magnetic field intensity are determined. Components E_z , H_x , H_y determine the electromagnetic field obtained as a result of diffraction of an electromagnetic wave of TE-polarization on the micro-objects. The existence and uniqueness of the solutions of the 2D problem of diffraction of the TE-polarized electromagnetic wave in an inhomogeneous micro-object is solved using the same procedure as that described in [30], so in this work it is not given.

3.2.2. TM-polarization

Using the equations (3.62) (3.65) and (3.66), we obtain the Helmholtz equation for the projection on the z -axis of the magnetic field strength vector

$$\frac{\partial}{\partial x} \left(\frac{1}{\varepsilon} \frac{\partial H_z}{\partial x} \right) + \frac{\partial}{\partial y} \left(\frac{1}{\varepsilon} \frac{\partial H_z}{\partial y} \right) + k_0^2 \mu H_z = 0. \quad (3.84)$$

Assuming from the conditions of the problem $\varepsilon_1 = \varepsilon_1(x, y)$, $\varepsilon_2 = \text{const}$, $\mu_1 = \mu_2 = 1$ and applying equation (3.84) to regions Ω_1, Ω_2 we obtain a system of equations:

$$\begin{cases} \left(\Delta + k_1^2 \right) H_z^{\text{in}} - \frac{1}{\varepsilon_1} \left(\frac{\partial \varepsilon_1}{\partial x} \frac{\partial H_z^{\text{in}}}{\partial x} + \frac{\partial \varepsilon_1}{\partial y} \frac{\partial H_z^{\text{in}}}{\partial y} \right) = 0, & (x, y) \in \Omega_1 \\ \left(\Delta + k_2^2 \right) H_z^{\text{ext}} = -g_2, & (x, y) \in \Omega_2 \end{cases}, \quad (3.85)$$

where $k_1^2 = k_0^2 \varepsilon_1(x, y)$, $k_2^2 = k_0^2 \varepsilon_2$, g_2 is a function describing the external sources.

The system (3.85) describes the 2D problem of diffraction of the TM-polarized electromagnetic wave on an object with an inhomogeneous refractive index.

From the first equation (3.71) in view of (3.65) and (3.66) we obtain the boundary condition:

$$\left. \frac{1}{\varepsilon_1} \frac{\partial H_z^{\text{in}}}{\partial n_1} \right|_S = - \left. \frac{1}{\varepsilon_2} \frac{\partial H_z^{\text{ext}}}{\partial n_2} \right|_S. \quad (3.86)$$

From the second equation of (4.71) we obtain

$$H_z^{\text{in}} \Big|_S = H_z^{\text{ext}} \Big|_S. \quad (3.87)$$

After a number of auxiliary calculations to convert the first equation of (3.85):

$$\begin{aligned} \frac{1}{\varepsilon_1} \Delta H_z^{\text{in}} - \frac{1}{\varepsilon_1^2} \left(\frac{\partial \varepsilon_1}{\partial x} \frac{\partial H_z^{\text{in}}}{\partial x} + \frac{\partial \varepsilon_1}{\partial y} \frac{\partial H_z^{\text{in}}}{\partial y} \right) &= \\ &= \frac{1}{\varepsilon_1} \Delta H_z^{\text{in}} + \left(\frac{\partial}{\partial x} \left(\frac{1}{\varepsilon_1} \right) \frac{\partial H_z^{\text{in}}}{\partial x} + \frac{\partial}{\partial y} \left(\frac{1}{\varepsilon_1} \right) \frac{\partial H_z^{\text{in}}}{\partial y} \right) = \frac{\partial}{\partial x} \left(\frac{1}{\varepsilon_1} \frac{\partial H_z^{\text{in}}}{\partial x} \right) + \\ + \frac{\partial}{\partial y} \left(\frac{1}{\varepsilon_1} \frac{\partial H_z^{\text{in}}}{\partial y} \right) &= \text{div} \left(\frac{1}{\varepsilon_1} \left(\mathbf{i} \frac{\partial H_z^{\text{in}}}{\partial x} + \mathbf{j} \frac{\partial H_z^{\text{in}}}{\partial y} \right) \right) = \text{div} \left(\frac{1}{\varepsilon_1} \text{grad } H_z^{\text{in}} \right). \end{aligned} \quad (3.88)$$

In view of the expression (3.88) the first equation of the system (3.85) becomes

$$\text{div} \left(\frac{1}{\varepsilon_1} \text{grad } H_z^{\text{in}} \right) + \frac{k_1^2}{\varepsilon_1} H_z^{\text{in}} = 0. \quad (3.89)$$

For the operator $\text{div} \left(\frac{1}{\varepsilon_1} \text{grad } H_z^{\text{in}} \right)$ we have the following Green's integral formula [51]:

$$\begin{aligned} \iint_{\Omega_1} \left\{ G_2 \operatorname{div} \left(\frac{1}{\varepsilon_1} \operatorname{grad} H_z^{\text{in}} \right) - H_z^{\text{in}} \operatorname{div} \left(\frac{1}{\varepsilon_1} \operatorname{grad} G_2 \right) \right\} dx dy = \\ = \oint_S \frac{1}{\varepsilon_1} \left(G_2 \frac{\partial H_z^{\text{in}}}{\partial n_1} - H_z^{\text{in}} \frac{\partial G_2}{\partial n_1} \right) dl, \end{aligned} \quad (3.90)$$

where G_2 is the Green's function for 2D light fields, satisfying the equation

$$\Delta G_2 = -k_2^2 G_2 - \delta(M, M_0). \quad (3.91)$$

Then for the operator $\operatorname{div} \left(\frac{1}{\varepsilon_1} \operatorname{grad} G_2 \right)$ taking into account equations (3.88) and (3.91) we have

$$\operatorname{div} \left(\frac{1}{\varepsilon_1} \operatorname{grad} G_2 \right) = \frac{1}{\varepsilon_1} \Delta G_2 - \frac{1}{\varepsilon_1^2} \nabla \varepsilon_1 \nabla G_2 = \frac{-k_2^2 G_2 - \delta(M, M_0)}{\varepsilon_1} - \frac{1}{\varepsilon_1^2} \nabla \varepsilon_1 \nabla G_2. \quad (3.92)$$

From equation (3.90) with (3.89) and (3.92) we obtain

$$\begin{aligned} \iint_{\Omega_1} \left\{ -\frac{k_1^2}{\varepsilon_1} H_z^{\text{in}} G_2 + \frac{k_2^2}{\varepsilon_1} H_z^{\text{in}} G_2 + \frac{H_z^{\text{in}} \delta(M, M_0)}{\varepsilon_1} - H_z^{\text{in}} \nabla \left(\frac{1}{\varepsilon_1} \right) \nabla G_2 \right\} dx dy = \\ = \oint_S \frac{1}{\varepsilon_1} \left(G_2 \frac{\partial H_z^{\text{in}}}{\partial n_1} - H_z^{\text{in}} \frac{\partial G_2}{\partial n_1} \right) dl, \end{aligned} \quad (3.93)$$

which implies

$$\begin{aligned} \oint_S \frac{1}{\varepsilon_1} \left(G_2 \frac{\partial H_z^{\text{in}}}{\partial n_1} - H_z^{\text{in}} \frac{\partial G_2}{\partial n_1} \right) dl + \iint_{\Omega_1} \frac{(k_1^2 - k_2^2)}{\varepsilon_1} H_z^{\text{in}} G_2 dx dy + \\ + \iint_{\Omega_1} H_z^{\text{in}} \nabla \left(\frac{1}{\varepsilon_1} \right) \nabla G_2 dx dy = \begin{cases} \frac{H_z^{\text{in}}}{\varepsilon_1}, & (x, y) \in \Omega_1 \\ 0, & (x, y) \in \Omega_2 \end{cases}. \end{aligned} \quad (3.94)$$

We apply Green's formula (3.90) for functions and taking into account the second of equations (3.85) and equation (3.91) and obtain

$$\frac{1}{\varepsilon_2} \iint_{\Omega_2} G_2 g_2 dx dy + \oint_S \left(\frac{G_2}{\varepsilon_2} \frac{\partial H_z^{\text{ext}}}{\partial n_2} - \frac{H_z^{\text{ext}}}{\varepsilon_2} \frac{\partial G_2}{\partial n_2} \right) dl = \begin{cases} 0, & (x, y) \in \Omega_1 \\ \frac{H_z^{\text{ext}}}{\varepsilon_2}, & (x, y) \in \Omega_2 \end{cases}. \quad (3.95)$$

Combining (3.94) and (3.95) taking into account the boundary conditions (3.86) and (3.87), we obtain a system of equations

$$\begin{aligned}
& \iint_{\Omega_1} (k_1^2 - k_2^2) \frac{H_z^{\text{in}} G_2}{\varepsilon_1} dx dy + H_{0z} + \iint_{\Omega_1} H_z^{\text{in}} \nabla \left(\frac{1}{\hat{a}_1} \right) \nabla G_2 dx dy + \\
& + \oint_S \left(\frac{\varepsilon_1 - \varepsilon_2}{\varepsilon_1 \varepsilon_2} \right) H_z^{\text{in}} \frac{\partial G_2}{\partial n_1} dl = \begin{cases} \frac{H_z^{\text{in}}}{\hat{a}_1}, & (x, y) \in \Omega_1 \\ \frac{H_z^{\text{ext}}}{\varepsilon_2}, & (x, y) \in \Omega_2 \end{cases}, \quad (3.96)
\end{aligned}$$

where $H_{0z} = \iint_{\Omega_2} G_2 g_2 dx dy$ is the given field produced by external sources.

Thus, the problem of diffraction of electromagnetic waves of TM-polarization is reduced to solving a Fredholm integral equation of the second kind with respect to the function $H_z^{\text{in}}(x, y)$. The existence and uniqueness of solutions is proved in [30] so in this work are not given. The Green function has the form (3.83).

By definition of the gradient $\text{grad } G_2 = \left(\frac{\partial G_2}{\partial x}, \frac{\partial G_2}{\partial y} \right)$. Since $\xi = \xi(x, y)$, then

$$\begin{aligned}
\frac{\partial G_2}{\partial x} &= \frac{\partial G_2}{\partial \xi} \frac{\partial \xi}{\partial x}, \\
\frac{\partial G_2}{\partial y} &= \frac{\partial G_2}{\partial \xi} \frac{\partial \xi}{\partial y}.
\end{aligned} \quad (3.97)$$

For the Hankel function the following relation holds

$$\frac{dH_0^{(1)}}{d\xi} = -H_1^{(1)}(\xi). \quad (3.98)$$

Given that $\frac{\partial \xi}{\partial x} = \frac{k_2^2(x-x')}{\xi}$, $\frac{\partial \xi}{\partial y} = \frac{k_2^2(y-y')}{\xi}$, from (3.83) (3.97) (3.98) we have

$$\text{grad } G_2 = -\frac{k_2^2 i}{4} \left(H_1^{(1)}(\xi) \frac{x-x'}{\xi}, H_1^{(1)}(\xi) \frac{y-y'}{\xi} \right). \quad (3.99)$$

Directional derivative in (3.96) with (3.99) can be calculated by the formula

$$\frac{\partial G_2}{\partial n_1} = n_1 \cdot \text{grad } G_2. \quad (3.100)$$

Field H_z , which is determined from the system (3.96), is substituted into equations (3.65) and (3.66) from which the components E_x, E_y of the vector of electric strength are determined. The components H_z, E_x, E_y determine by the electromagnetic field, resulting from diffraction of electromagnetic wave of TM-polarization on a micro-object.

3.2.3. Application of finite element method for solving integral equation

To solve the integral equations of the systems (3.81) and (3.96) we use the finite element method in which by expanding the required fields with respect the basis of interpolating functions these equations were reduced to ???. The system of interpolating functions was represented by linear functions inside cells obtained in discretization of region Ω_1 . The linear interpolation functions within the discretization grid have the form [13]

$$\psi_m(x,y) = \begin{cases} 1 - \frac{x_m - x}{\Delta} - \frac{y_m - y}{\Delta}, & (x,y) \in \Omega_1(\Delta_1) \\ 1 - \frac{x_m - x}{\Delta}, & (x,y) \in \Omega_1(\Delta_2) \\ 1 + \frac{y_m - y}{\Delta}, & (x,y) \in \Omega_1(\Delta_3) \\ 1 + \frac{x_m - x}{\Delta} + \frac{y_m - y}{\Delta}, & (x,y) \in \Omega_1(\Delta_4) \\ 1 + \frac{x_m - x}{\Delta}, & (x,y) \in \Omega_1(\Delta_5) \\ 1 - \frac{y_m - y}{\Delta}, & (x,y) \in \Omega_1(\Delta_6) \end{cases}, \quad (3.101)$$

where Δ is the step of the ???, as shown in Fig. 3.15. $\Delta_i, i = \overline{1,6}$ are the triangular cells of the neighborhood of the current point m . In Fig. 3.15 $(p + 1)$ is the number of discretization nodes along the x axis.

For the case of TE-polarization of the incident wave, expansion in the basis (3.101) takes the form

$$E_z^{in}(x,y) = \sum_{m=1}^N C_m \psi_m(x,y), \quad (3.102)$$

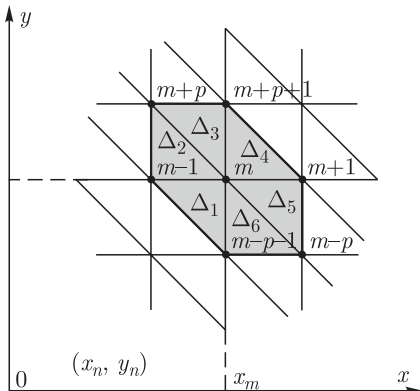


Fig. 3.15. A fragment of triangulation of region Ω_1 .

where C_m are unknown coefficients.

Substituting (3.102) in the integral equation of (3.81), we obtain the ??? for the unknown C_m

$$\sum_{m=1}^N C_m D_{mn} = E_{0n}, \quad (3.103)$$

where

$$D_{mn} = \psi_m(x_n, y_n) - \iint_{\Omega_1} (k_1^2 - k_2^2) \psi_m(x', y') \cdot G_2(x_n, y_n; x', y') dx' dy',$$

$$E_{0n} = E_{0z}(x_n, y_n). \quad (3.104)$$

For the case of TM-polarized incident wave expansion in the basis (3.101) takes the form

$$H_z^{in}(x, y) = \sum_{m=1}^N C_m \psi_m(x, y), \quad (3.105)$$

where C_m are unknown coefficients.

Substituting (3.105) in the integral equation of (4.96), we obtain the ??? for the unknown

$$\sum_{m=1}^N C_m D_{mn} = H_{0n}, \quad (3.106)$$

where

$$D_{mn} = \begin{cases} \frac{\psi_m(x_n, y_n)}{\varepsilon_1(x_n, y_n)} - \iint_{\Omega_1} (k_1^2(x', y') - k_2^2) \frac{\Psi_m(x', y')}{\varepsilon_1(x', y')} G_2(x', y'; x_n, y_n) dx' dy' - \\ - \iint_{\Omega_1} \psi_m(x', y') \nabla \left(\frac{1}{\varepsilon_1(x', y')} \right) \nabla G_2(x', y'; x_n, y_n) dx' dy', & (x, y) \in \Omega_Q \setminus S \\ \frac{\Psi_m(x_n, y_n)}{\varepsilon_1(x_n, y_n)} - \iint_{\Omega_1} (k_1^2(x', y') - k_2^2) \frac{\Psi_m(x', y')}{\varepsilon_1(x', y')} G_2(x', y'; x_n, y_n) dx' dy' - \\ - \iint_{\Omega_1} \psi_m(x', y') \nabla \left(\frac{1}{\varepsilon_1(x', y')} \right) \nabla G_2(x', y'; x_n, y_n) dx' dy' - \\ - \oint_S \mathbf{n} \nabla G_2(x', y'; x_n, y_n) \psi_m(x', y') \left(\frac{\varepsilon_1(x', y') - \varepsilon_2}{\varepsilon_1(x', y') \varepsilon_2} \right) dl, & (x, y) \in S \end{cases}$$

$$H_{0n} = \frac{H_{0z}(x_n, y_n)}{\varepsilon_2}. \quad (3.107)$$

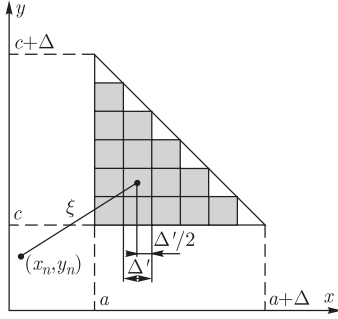


Fig. 3.16. Discretization of the triangular element of the ??? grid (Fig. 3.15) for numerical integration.

Since the integrands of the integrals in (3.104) and (3.107) have a complicated form, then their integrals are numerically implemented for each of the six triangles of the current node m . In the case where $m = n$ the Neumann function $Y_0(x_n, y_n; x_m, y_m)$, which is part of the component of the function G_2 has a feature, i.e. tends to $-\infty$. To calculate the function Y_0 in the neighborhood we need more detailed discretization of the triangular element formed by the ??? grid, shown in Fig. 3.16.

Here (a, c) are the coordinates of the point from which integration starts, and Δ' is the step of the inner ??? grid, shown in Fig. 3.16. The element is divided into squares, and triangles, as shown in Fig. 3.16. The integration in (3.104) is carried out as follows: function $(k_1^2 - k_2^2) \psi_m$ is integrated analytically for each square (in each square k_1 and k_2 are assumed constant), and the Green's function G_2 which is a function of distance ξ , is assumed to be constant for each square. Integrals for the area in (3.107) are calculated in a similar way, and to calculate the integral along the contour sections with the same step Δ' are used instead of squares.

Matrices D_{mn} of the systems (3.103), (3.106) are symmetric, fully populated with the dominant main diagonal. Symmetry D_{mn} is due to the fact that the Green function G_2 is an even function of the distance between the observation point n and the current point m . The prevalence of the main diagonal is due to the fact that the Neumann function Y_0 has a feature??? at the origin. Indeed, this feature occurs when $n = m$, i.e. when calculating the diagonal elements. For a single observation point n enumeration??? happens through all the points of region Ω_1 , that is in the same row of the matrix D_{mn} there are N elements (N is the number of points in the region Ω_1). Thus, the resultant ??? are of order N . To solve the ??? we used the Gauss method for complex numbers. The number of arithmetic operations performed in the solution of ??? can be estimated as $\approx (2/3)N^3$ [52].

For the case of TE-polarization by solving a system of equations (3.103) we obtain the complex coefficients C_m , $m = 1, N$ which are then substituted into the second equation (3.118) to determine the field in the outer region Ω_2 :

$$E_z^{\text{ext}}(x_n, y_n) = E_{0z}(x_n, y_n) + \sum_{m=1}^N C_m \cdot \iint_{\Omega_1} (k_1^2 - k_2^2) \psi_m(x', y') G_2(x_n, y_n; x', y') dx' dy'. \quad (3.108)$$

Solving the system of equations (3.106) for the case of TM-polarization, we obtain the complex coefficients C_m , $m = 1, N$ which are then substituted into the second equation (3.96) to determine the field in the outer region:

$$\begin{aligned}
 \frac{H_z^{\text{ext}}(x_n, y_n)}{\varepsilon_2} &= H_{0z}(x_n, y_n) + \sum_{m=1}^N C_m \cdot \\
 &\cdot \left[\iint_{\Omega_1} (k_1^2 - k_2^2) \frac{\Psi_m(x', y') G_2(x_n, y_n; x', y')}{\varepsilon_1(x', y')} dx' dy' + \right. \\
 &+ \iint_{\Omega_1} \Psi_m(x', y') \nabla \left(\frac{1}{\varepsilon_1(x', y')} \right) \nabla G_2(x_n, y_n; x', y') dx' dy' + \\
 &\left. + \oint_S \left(\frac{\varepsilon_1(x', y') - \varepsilon_2}{\varepsilon_1(x', y') \varepsilon_2} \right) \Psi_m(x', y') \frac{\partial G_2(x_n, y_n; x', y')}{\partial n_1} dl \right].
 \end{aligned} \tag{3.109}$$

The described method has several advantages and disadvantages compared with other methods. In contrast to the FEM, in Gallagher's formulation [13] the integral equation method does not require specification of boundary conditions and can operate with objects having an arbitrary boundary. However, the use of Green's function considerably complicates the numerical implementation. This method also does not require the calculation of normal and tangential derivatives along the contour of the object from the light field, which distinguishes it from the finite element method [13] and the hybrid finite element method [53]. At the same time, the hybrid method computes several times faster (for the given parameters of the problem and discretization) than the method of integral equations, as in the hybrid method the ??? matrix is tridiagonal, and in this method it is completely filled out (which requires a significant amount of memory in numerical experiments). The method of the integral equation allows the calculation of the diffraction on both homogeneous and heterogeneous objects, and also, importantly, on the combination of several objects, with no need to introduce an artificial field, covering all scattering objects.

3.2.4. Convergence of the approximate solution

The numerical experiment showed that the method has a convergence. To do this, the test object was a homogeneous dielectric cylinder with permittivity $\varepsilon_1 = 4$ and the square cross-section of the size equal to the length of the incident wave. The cylinder was illuminated by a TE-polarized plane electromagnetic wave with the wavelength $\lambda = 1$ mm. The external environment was vacuum with the permittivity $\varepsilon_2 = 1$. The diffraction pattern with the size of 5×5 mm is shown in Fig. 3.17:

The main discretization grid was 100×100 nodes. Depending on the number of nodes of discretization of the fine grid the value of the maximum in the intensity

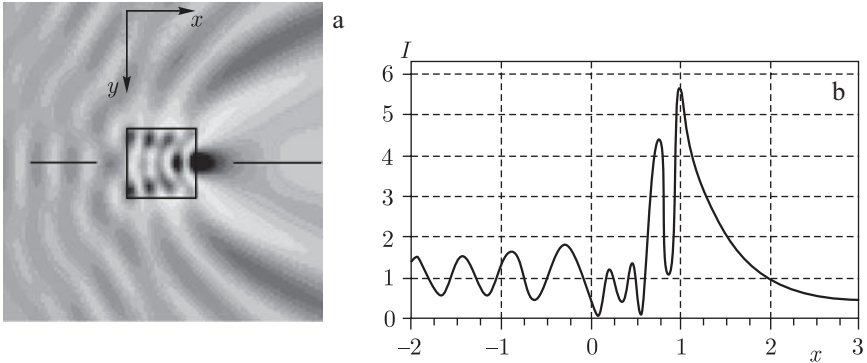


Fig. 3.17. Diffraction of a plane TE-wave by a dielectric cylinder with a square cross-section: a) the intensity distribution in the plane XY ; b) cross-section of the intensity of X

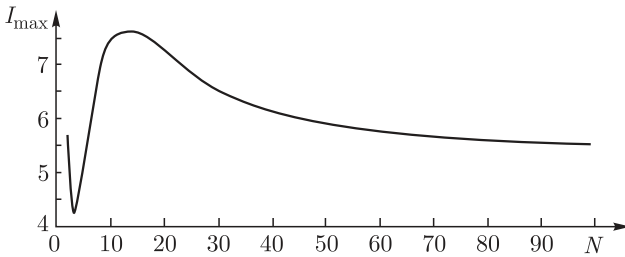


Fig. 3.18. Dependence of the maximum intensity in the 2D pattern of diffraction of a plane TE-wave on a square with the side λ on the number of nodes N of discretization of a 'fine' grid between two adjacent nodes of the main grid.

distribution in the plane XY changes. As the number of nodes of the fine grid increases the maximum value asymptotically approaches a constant value (Fig. 3.18): Fig. 3.17 corresponds to the number of nodes of the fine grid $N = 100$.

3.2.5. The diffraction of light by cylindrical microlenses

The diffraction of light on microlens was analyzed using a collecting lens with a radius of curvature $R = 2.5 \mu\text{m}$ ($3 \mu\text{m}$ aperture of the lens), the refractive index of $n = 2$ and a thickness of $0.5 \mu\text{m}$. A plane wave with the length $\lambda = 1 \mu\text{m}$ impacted on the lens. The diffraction pattern had the dimensions $5 \times 5 \mu\text{m}$ with discretization grid of 100×100 nodes. The fine grid – 50 nodes on the distance between two nodes of the main grid. The aim of light diffraction study on the microlens was to find its focus and compare the results with the geometrical optics approximation of a thin lens. A study was conducted of the impact of its orientation to the incident radiation of flat and convex sides on the focus position.

The experimental results are shown in Figs. 3.19 and 3.20.

As can be seen from Figs. 3.19 and 3.20, the total diffraction pattern at different orientations of the lens has a different intensity distribution in the plane XY . However,

from Fig. 3.19c and Fig.3.20c show in that the the intensity at the focus is almost identical and differs by no more than 5%.

From the geometric optics approximation for a thin lens it follows that its focal length is equal to

$$f = \frac{R_1 R_2}{(n-1)(R_1 + R_2)}, \quad (3.110)$$

where R_1 and R_2 are the radii of curvature of the surfaces of the lens, n is the refractive index of the lens. Given that $R_1 = \infty$, the formula (3.110) becomes

$$f = \frac{R_2}{(n-1)}. \quad (3.111)$$

It follows from (3.111), taking into account the lens parameters, that the focal length is $f = 2.5 \mu\text{m}$.

From Fig. 3.19b $f \approx 3.05 \mu\text{m}$, which is different from the theoretical result by 22%, and from Fig. 3.20b $f \approx 3.25 \mu\text{m}$, which is different from the theoretical result by 30%. We conclude that the diffraction of light on the microlens causes shift of the focus of the lens, which depends on the orientation of the lens in relation to the incident plane wave.

Figures 3.19b and Fig. 3.20b also show that the type of diffraction pattern inside and in front of the lenses is significantly different: at the reflection of the plane face of the lens (Fig. 3.19b) there is a local maximum of intensity whose value is 1.3 times larger than the focus.

Microlenses with a continuous profile represent a significant challenge to make, so the question: how accurately can these lenses can be approximated by binary lenses? is of considerable importance.

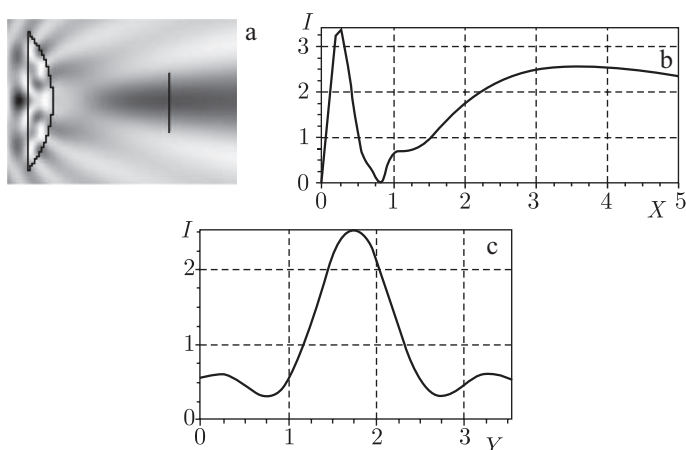


Fig. 3.19. Diffraction of a plane TE-wave on a microlens oriented with the flat edge to the incident wave: a) the intensity distribution in the plane XY ; b) cross-section of the intensity with respect to X , c) cross-section of the intensity with respect to Y .

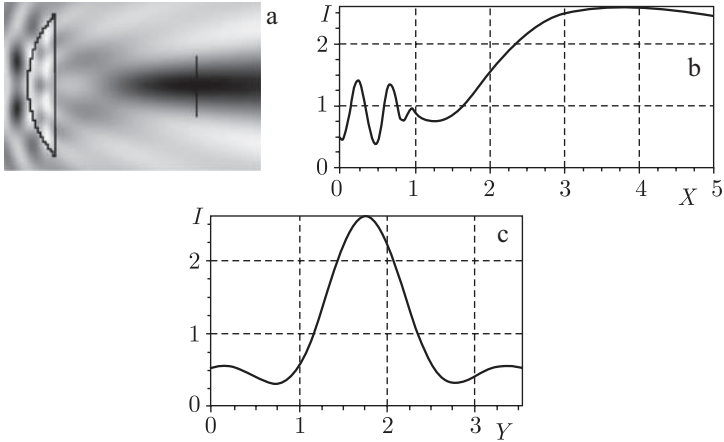


Fig. 3.20. Diffraction of a plane TE-wave by a microlens oriented with the convex surface to the incident wave: a) the intensity distribution in the plane XY ; b) cross-section of intensity with respect to X , c) cross-section of intensity with respect to Y .

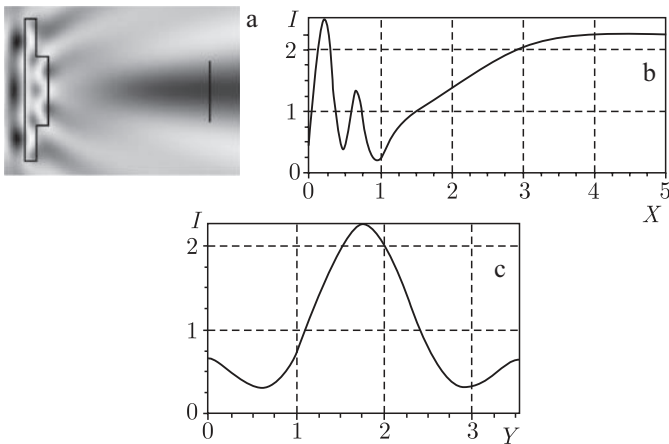


Fig. 3.21. Diffraction of a plane TE wave by a binary microlens: a) the intensity distribution in the plane XY ; b) cross-section of intensity with respect to X , c) cross-section of intensity with respect to Y .

Figure 3.21 shows the diffraction of a plane wave on a binary microlens. Its parameters are the same as in the previous example.

Figures 3.21a and 3.21b show that the focal length of a binary lens is 18–26% greater than the focal length of the ordinary lens. A large part of the energy is reflected back and the focal length increased to about $3.85 \mu\text{m}$. The width of the intensity maximum in the cross section for the X -axis of the focus increased compared with the continuous lens by $\approx 2.3 \mu\text{m}$ against $2 \mu\text{m}$ for the normal lens (Fig. 3.19c); the maximum light intensity at the focus of a binary microlens was $\approx 88\%$ of the maximum intensity of the continuous microlens (Fig. 3.19c).

Note that the numerical results presented in this section differ from those obtained in the hybrid method in [44] also by the fact that the aperture of the lens was 3λ , while in [53] the aperture was 8λ .

3.2.6. Diffraction of light on microscopic objects with a piecewise-uniform refractive index

A feature of the modification the finite element method for solving the Fredholm integral equation of the second kind, discussed in this chapter, is that it allows the calculation of diffraction not only on homogeneous objects, but also on objects with a piecewise-uniform refractive index. In other words, if the piecewise-homogeneous region Ω_1 can be divided into a finite number N of homogeneous subdomains Ω_{1i} , then for the case of TE-polarization the system (3.81) takes the form

$$\sum_{i=1}^N \iint_{\Omega_{1i}} (k_{1i}^2 - k_2^2) E_z^{\text{in}} G_2 dx dy + E_{0z} = \begin{cases} E_z^{\text{in}}, (x, y) \in \Omega_1 \\ E_z^{\text{ext}}, (x, y) \in \Omega_2 \end{cases}. \quad (3.112)$$

To test this assertion, the numerical results of the diffraction problem of a plane TE-polarized electromagnetic wave, obtained by the considered method and the analytical method described in [54, 55, 56], were compared.

Figure 3.22 shows the diffraction pattern of a plane TE-wave with a length $\lambda = 1 \mu\text{m}$ for a two-layer dielectric circular cylinder with the characteristics $r_1 = 0.25 \mu\text{m}$, $r_2 = 0.5 \mu\text{m}$, $\varepsilon_1 = 2.25$; $\varepsilon_2 = 4$. Outer space – a vacuum. The dimensions of the diffraction pattern were $3.33 \times 3.33 \mu\text{m}$. The sampling grid had 200×200 nodes.

In Fig. 3.22b the intensity curve, displayed by black colour, corresponds to the analytical solution [56], while the gray curve corresponds to the investigated method (3.112). For the above mentioned parameters of the problem the compared results differ by 4–5%. This allows us to conclude that the method is suitable for calculating diffraction problems for piecewise-homogeneous (in the general case of inhomogeneous) micro-objects.

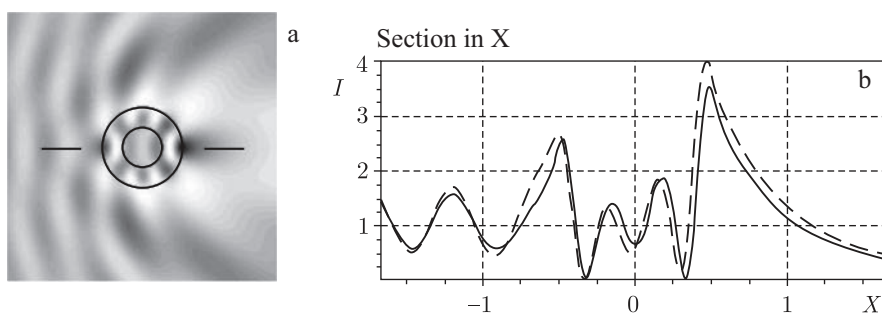


Fig. 3.22. Diffraction of a plane TE-wave on a two-layer microlenses: a) the intensity distribution in the plane XY ; b) cross-section of intensity with respect to X .

Consider now one of the simplest examples of diffraction of light on piecewise-homogeneous microscopic objects – the diffraction of light on layered films.

The investigated object was a plate with the following parameters (Fig. 3.23):

- dimensions: $0.5 \times 3 \mu\text{m}$;
- the refractive index:
- left layer with thickness $0.25 \mu\text{m}$ $n_{1l} = 2$;
- right layer with thickness $0.25 \mu\text{m}$; $n_{1r} = 1.5$;
- the external environment $n_2 = 1$;
- the wavelength of incident radiation $\lambda = 1 \mu\text{m}$,
- the number of counts in the sampling grid 200×200 ;
- the size of the outer region $10 \times 10 \text{ mm}$.

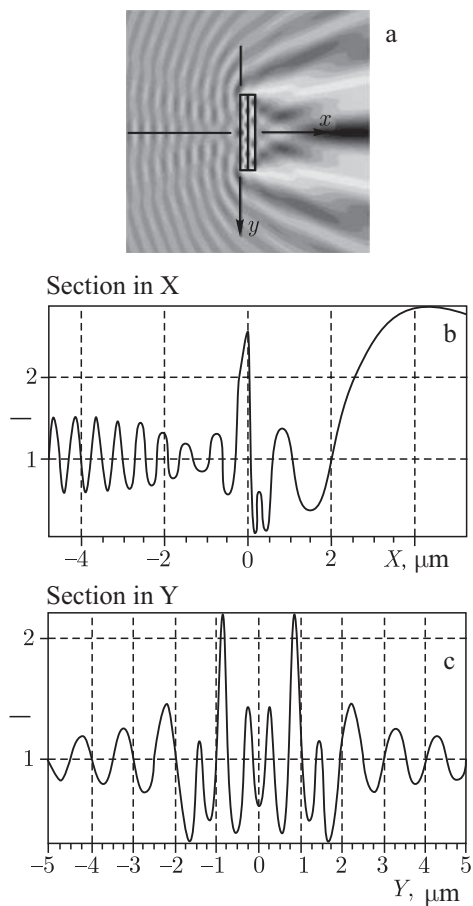


Fig. 3.23. Diffraction of a plane TE-wave by a layered film: a) the light intensity distribution in the plane XY ; b) cross-section of intensity in X , c) cross-section of intensity in Y .

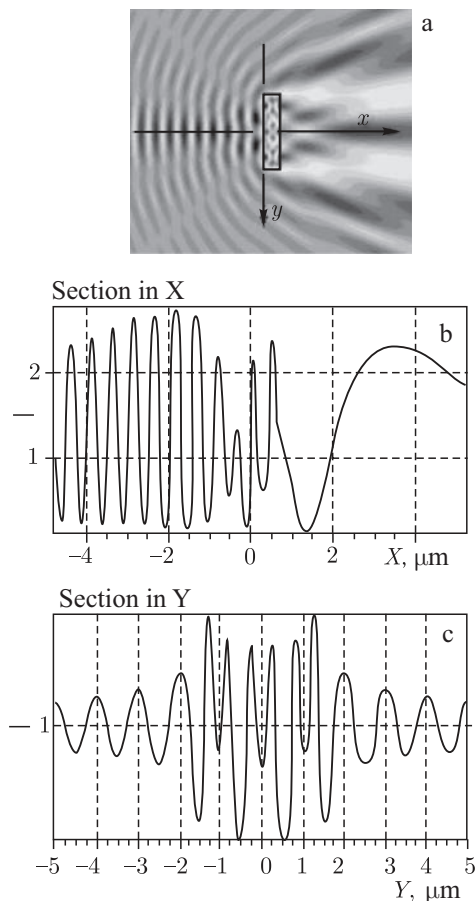


Fig. 3.24. Diffraction of a plane TE-wave on a homogeneous film: a) the light intensity distribution in the plane XY ; b) cross-section of intensity in X , c) cross-section of intensity in Y .

Next, a layered film was replaced with a uniform refractive index with the same dimensions as the previous model (Fig. 3.24).

Figure 3.23b and 3.24b show that the layered film has a higher transmittance than the homogeneous film, and the bleaching effect was observed there. This suggests that by replacing the homogeneous object by a piecewise-uniform one we can achieve the required value of the reflection and transmission, which is very important for the design of micro-lenses and other micro-optics objects.

It is interesting to note that both models have the focusing properties, such as microlenses, and the magnitude of the maximum intensity at the focus can be controlled by the choice of layers with different refractive indices. In Fig. 3.23b the maximum intensity at the focus is 3 and in Fig. 3.24b it is 2.4.

3.3. Diffraction of light on inhomogeneous dielectric cylinders

Among the many tasks of light scattering on microscopic objects special attention is paid to the solution of axisymmetric problems of diffraction of electromagnetic waves on bodies of revolution [57–61]. For example, in [62] to solve the scattering problem on 3D axisymmetric particles, the authors suggested the method of separation of electromagnetic fields into two parts: axisymmetric, independent of the azimuthal angle, and asymmetric, whose average over this angle is zero. The scattering problem is considered separately for each of these parts. At the same time, special selection is made of scalar potentials associated with the azimuthal components of the electromagnetic fields used for the axisymmetric part of these fields. For the asymmetric part we used the superposition of Debye potentials and vertical components of the Hertz vector. The formulation of the problem is reduced to solving an integral equation, which requires large computational costs.

In [63] the analytic solution of near-field diffraction on homogeneous metallic and dielectric circular cylinders in the vicinity of the dielectric surface is studied. In [64] the problem of a more general form, where a homogeneous circular cylinder is immersed in a layered medium, is solved.

In [65], the modification of the method of discrete sources was proposed for the two-dimensional problem of diffraction of a plane TE-polarized electromagnetic waves on a two-layer circular dielectric cylinder or a metal cylinder with a dielectric coating.

In [66] the electromagnetic scattering by a multilayer gyrotropic bianisotropic circular cylinder for TE-/TM-polarized incident plane waves was investigated using the method of eigenfunction expansion. Numerical results are presented for a three-layer cylinder.

In [67–70] in the framework of geometrical optics the authors obtained analytical expressions for the dependence of the refractive index on the radial coordinate of gradient optical elements with spherical and transverse cylindrical symmetry (when an infinitely long lateral surface is perpendicular to the direction of incidence of the electromagnetic wave). Note that the Luneberg lens [69] is also used as a lens antenna for UHF band radio waves [71]. The Luneberg lens focuses the beam of parallel rays to a point on the surface. The inner Luneberg lens [68] focuses a beam of parallel rays in a given internal point lying on a diameter parallel to the incident rays between the centre and the far surface of the lens. The generalized Luneberg lens [67] focuses the incident beam of parallel rays to a point behind the lens, which lies on the continuation of the diameter parallel to the incident rays. In this case, the dependence of the refractive index on the radial variable no longer has an explicit analytical dependence, and is expressed in the form of integral relations. The Eaton-Lippmann lens [70] is a dielectric gradient optical element having a spherical or transverse cylindrical symmetry, which reflects back all the rays falling on it. An explicit analytical dependence of the refractive index on the coordinate for the Eaton-Lippmann lens has a singularity at the origin (in the centre of the lens), which provides back reflection of rays incident at the centre of the lens.

Traces of light rays in all the lenses have been studied well enough. This chapter discusses the passage of the electromagnetic wave through these gradient optical elements, in the case where the radius of the lens is the same (or similar) with the wavelength. In this resonance case, the beam description of diffraction of light is no longer valid and the question arises about the extent of change in the focusing and reflection properties of the given gradient elements.

The analysis of electromagnetic wave diffraction on the gradient cylindrical optical elements, the refractive index of which has a transverse cylindrical symmetry, can be carried out using the method of integral equations described in section 3.2. The numerical solution of Fredholm integral equations of the second kind is generally conducted using methods for solving systems of linear algebraic equations (one of these methods – the finite element method – was also discussed in chapter 1). However, to obtain sufficient accuracy of the system we should consider high-order equations with completely filled matrices, which requires a considerable amount of computing time and a large amount of computer memory. In this connection there was a need to develop a method that would solve the problem of electromagnetic wave diffraction on a transparent body in a short time frame and without significant computational costs.

In this chapter, the method of separation of variables is used to develop the recurrent analytical method for calculating the diffraction field with TE- and TM-polarizations, in the event of the incidence of the electromagnetic wave on an inhomogeneous dielectric infinite circular cylinder whose generating line extends along the axis z , while the plane (x, y) is the plane of incidence. The heterogeneity of the cylinder is approximated by a piecewise-constant function, and the circular section of the cylinder at the same time will have N concentric rings with constant values of the refractive index within each ring (Fig. 3.25). The method is based on the decomposition of the projection on the z -axis of the vectors of the electric (for TE-polarization) or magnetic (for TM-polarization) fields within each homogeneous ring into a series of cylindrical functions with unknown coefficients. The coefficients themselves are determined from the boundary conditions imposed on the field and their radial derivatives on the lines of discontinuities of the refractive index.

3.3.1. Solution of the problem of diffraction of an arbitrary wave on a cylindrical multilayer dielectric cylinder by separation of variables

Figure 3.25 schematically shows the section of an N -layered circular cylinder in each layer of which the refractive index is constant. The generator of the infinite cylinder is elongated along the axis z , and the plane of incidence of a plane monochromatic electromagnetic wave coincides with the plane (x, y) . In this case, the system of six Maxwell equations splits into two independent systems of three equations: for TE-polarization the system of three equations includes the projections of the vectors of the strength of electric and magnetic fields (E_x, H_x, H_y) , for TM-polarization the system is formed by the projections of the vectors (H_z, E_x, E_y) . For TE-polarization

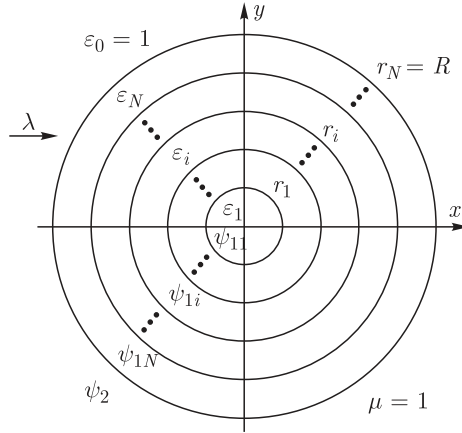


Fig. 3.25. Multilayer dielectric cylinder.

projection E_z satisfies the Helmholtz equation, and the projections H_x and H_y are expressed through E_z , and for TM-polarization, projection H_z satisfies the Helmholtz equation, and the projections E_x and E_y are expressed by H_z .

Thus, to solve the problem we need to solve the Helmholtz equation for the projections E_z and H_z . If we place the centre of the coordinate system (x, y) at the centre of the circular cylinder, then the problem can be solved in cylindrical coordinates (r, φ) : $x = r \cos \varphi$, $y = r \sin \varphi$. It is known that partial solutions of the Helmholtz equation in cylindrical coordinates are cylindrical functions, so any solution of the Helmholtz equation in the variables (r, φ) , where the refractive index is constant, can be represented as a linear combination of independent cylindrical functions.

TE-polarization

In this section we introduce the notation $E_z = \psi$.

The field amplitude in the inner circle ($0 \leq r \leq r_1$) is represented as a series of Bessel functions (Rayleigh series):

$$\psi_{11} = \sum_{m=-\infty}^{+\infty} C_{1m} J_m(k\sqrt{\varepsilon_1}r) \cos m\varphi. \quad (3.113)$$

The field inside the j -th ring of the dielectric is represented as a series of Bessel and Neumann functions:

$$\psi_{1j} = \sum_{m=-\infty}^{+\infty} \left[C_{(2j-2)m} J_m(k\sqrt{\varepsilon_j}r) + C_{(2j-1)m} Y_m(k\sqrt{\varepsilon_j}r) \right] \cos m\varphi, \quad (3.114)$$

where $r_{j-1} < r \leq r_j$, $j = \overline{2, N}$. Here $r_N = R$.

The amplitude of the field outside the dielectric is represented as a series of Hankel functions of the second kind, since they satisfy the Sommerfeld radiation condition:

$$\psi_2 = \psi_0 + \sum_{m=-\infty}^{+\infty} C_{2Nm} H_m^{(2)}(kr) \cos m\varphi, \quad (3.115)$$

where $r > R$. Here we assume that in the freespace the permittivity is equal to unity $\varepsilon_2 = 1$.

In equation (3.115) $\psi_0 = \exp(-ikx) = \exp(-ikr \cos \varphi)$ is the amplitude of the incident plane wave of unit intensity.

To find the unknown coefficients in the series (3.113)–(3.115) we use the boundary conditions. Equating the fields themselves and their radial derivatives at the radii of the jumps of the refractive index r_j , we obtain a system of equations:

$$\begin{cases} \psi_{1j} \Big|_{r_j} = \psi_{1(j+1)} \Big|_{r_j} \\ \frac{\partial \psi_{1j}}{\partial r} \Big|_{r_j} = \frac{\partial \psi_{1(j+1)}}{\partial r} \Big|_{r_j} \end{cases}, j = \overline{1, N-1}, \quad (3.116)$$

$$\begin{cases} \psi_{1N} \Big|_R = \psi_2 \Big|_R \\ \frac{\partial \psi_{1N}}{\partial r} \Big|_R = \frac{\partial \psi_2}{\partial r} \Big|_R \end{cases}.$$

For the expansion of ψ_0 into a series in respect of Bessel functions we use the series connected with the generating function [50]:

$$\begin{aligned} \cos(z \cos \theta) &= J_0(z) + 2 \sum_{k=1}^{\infty} (-1)^k J_{2k}(z) \cos(2k\theta), \\ \sin(z \cos \theta) &= 2 \sum_{k=0}^{\infty} (-1)^k J_{2k+1}(z) \cos[(2k+1)\theta]. \end{aligned} \quad (3.117)$$

For a plane wave from the equations (4.117) it follows:

$$\begin{aligned} \psi_0 \Big|_{r=R} &= \cos(kR \cos \varphi) - i \sin(kR \cos \varphi) = \\ &= J_0(kR) + 2 \sum_{m=1}^{\infty} (-1)^m J_{2m}(kR) \cos(2m\varphi) - \\ &\quad - 2i \sum_{m=0}^{\infty} (-1)^m J_{2m+1}(kR) \cos[(2m+1)\varphi] \end{aligned} \quad (3.118)$$

Given that $(-1)^m = (-i)^{2m}$ and $-i \cdot (-1)^m = (-i)^{2m+1}$ from equation (3.118) we have

$$\begin{aligned}
\psi_0|_{r=R} &= J_0(kR) + 2 \sum_{m=1}^{\infty} (-i)^{2m} J_{2m}(kR) \cos(2m\varphi) + \\
&+ 2 \sum_{m=0}^{\infty} (-i)^{2m+1} J_{2m+1}(kR) \cos[(2m+1)\varphi] = \quad (3.119) \\
&= J_0(kR) + 2 \sum_{m=1}^{\infty} (-i)^m J_m(kR) \cos m\varphi
\end{aligned}$$

We check the parity of the function $(-i)^m J_m(kR) \cos m\varphi$:

$$(-i)^{-m} J_{-m}(kR) \cos(-m\varphi) = \frac{1}{(-i)^m} (-1)^m J_m(kR) \cos m\varphi = (-i)^m J_m(kR) \cos m\varphi.$$

Here we use the property $J_{-m}(kR) = (-1)^m J_m(kR)$.

Since the function under the sum in equation (3.119) is even, then the expansion of a plane wave in the series becomes

$$\begin{aligned}
\psi_0|_{r=R} &= \sum_{m=-\infty}^{+\infty} (-i)^m J_m(kR) \cos m\varphi, \quad (3.120) \\
\frac{\partial \psi_0}{\partial r} \Big|_{r=R} &= k \sum_{m=-\infty}^{\infty} (-i)^m J'_m(kR) \cos m\varphi.
\end{aligned}$$

When $j = 1$ taking into account (3.113) and (3.114) from (3.116) we have:

$$\left\{ \begin{aligned}
&\sum_{m=-\infty}^{+\infty} C_{1m} J_m(k\sqrt{\varepsilon_1} r_1) \cos m\varphi = \\
&= \sum_{m=-\infty}^{+\infty} \left[C_{2m} J_m(k\sqrt{\varepsilon_2} r_1) + C_{3m} Y_m(k\sqrt{\varepsilon_2} r_1) \right] \cos m\varphi \\
&\sqrt{\varepsilon_1} \sum_{m=-\infty}^{+\infty} C_{1m} J'_m(k\sqrt{\varepsilon_1} r_1) \cos m\varphi = \\
&= \sqrt{\varepsilon_2} \sum_{m=-\infty}^{+\infty} \left[C_{2m} J'_m(k\sqrt{\varepsilon_2} r_1) + C_{3m} Y'_m(k\sqrt{\varepsilon_2} r_1) \right] \cos m\varphi
\end{aligned} \right. \quad (3.121)$$

At $j = 2, N-1$ taking into account (3.114) from (3.116) we have:

$$\begin{cases}
\sum_{m=-\infty}^{+\infty} \left[C_{(2j-2)m} J_m(k\sqrt{\varepsilon_j} r_j) + C_{(2j-1)m} Y_m(k\sqrt{\varepsilon_j} r_j) \right] \cos m\varphi = \\
= \sum_{m=-\infty}^{+\infty} \left[C_{2jm} J_m(k\sqrt{\varepsilon_{j+1}} r_j) + C_{(2j+1)m} Y_m(k\sqrt{\varepsilon_{j+1}} r_j) \right] \cos m\varphi \\
\sqrt{\varepsilon_j} \sum_{m=-\infty}^{+\infty} \left[C_{(2j-2)m} J'_m(k\sqrt{\varepsilon_j} r_j) + C_{(2j-1)m} Y'_m(k\sqrt{\varepsilon_j} r_j) \right] \cos m\varphi = \\
= \sqrt{\varepsilon_{j+1}} \sum_{m=-\infty}^{+\infty} \left[C_{2jm} J'_m(k\sqrt{\varepsilon_{j+1}} r_j) + C_{(2j+1)m} Y'_m(k\sqrt{\varepsilon_{j+1}} r_j) \right] \cos m\varphi
\end{cases} \quad (3.122)$$

When $j = N$, taking into account (3.114), (3.115) and (3.120) from (3.116) we have:

$$\begin{cases}
\sum_{m=-\infty}^{+\infty} \left[C_{(2N-2)m} J_m(k\sqrt{\varepsilon_N} r_N) + C_{(2N-1)m} Y_m(k\sqrt{\varepsilon_N} r_N) \right] \cos m\varphi = \\
= \sum_{m=-\infty}^{+\infty} (-i)^m J_m(kr_N) \cos m\varphi + \sum_{m=-\infty}^{+\infty} C_{2Nm} H_m^{(2)}(kr_N) \cos m\varphi \\
\sqrt{\varepsilon_N} \sum_{m=-\infty}^{+\infty} \left[C_{(2N-2)m} J'_m(k\sqrt{\varepsilon_N} r_N) + C_{(2N-1)m} Y'_m(k\sqrt{\varepsilon_N} r_N) \right] \cos m\varphi = \\
= \sum_{m=-\infty}^{+\infty} (-i)^m J'_m(kr_N) \cos m\varphi + \sum_{m=-\infty}^{+\infty} C_{2Nm} H_m^{(2)}(kr_N) \cos m\varphi
\end{cases} \quad (3.123)$$

If the cylinder does not fall flat, and an arbitrary wave satisfying the Helmholtz equation, the function can be written as [72]:

$$\psi_0(r, \varphi) = \int_{-\pi}^{\pi} h(\theta) \exp[ikr \cos(\varphi - \theta)] d\theta, \quad (3.124)$$

where $h(\theta)$ is an arbitrary function. We expand the exponent in the integrand of (3.124) in a series of cylindrical functions:

$$\exp[ikr \cos(\varphi - \theta)] = \sum_{m=-\infty}^{+\infty} (-i)^m J_m(kr) e^{im(\varphi - \theta)}, \quad (3.125)$$

then

$$\psi_0(r, \varphi) = \sum_{m=-\infty}^{+\infty} (-i)^m J_m(kr) e^{im\varphi} \int_{-\pi}^{\pi} e^{-im\theta} h(\theta) d\theta. \quad (3.126)$$

If $h(\theta)$ is an even and real function, then its Fourier transform $A_m = \int_{-\pi}^{\pi} e^{-im\theta} h(\theta) d\theta$ is also an even and real function. Thus, for any even real function we can write:

$$\psi_0(r, \varphi) = \sum_{m=-\infty}^{+\infty} (-i)^m A_m J_m(kr) \cos m\varphi, \quad (3.127)$$

where $A_m = \int_{-\pi}^{\pi} h(\theta) \cos m\theta d\theta$.

A plane wave propagating along the optical axis is described by the function $h(\theta) = \delta(\theta)$. In this case, $A_m = 1$ for any m .

In view of (3.127), system (3.123) takes the form:

$$\left\{ \begin{aligned} & \sum_{m=-\infty}^{+\infty} \left[C_{(2N-2)m} J_m(k\sqrt{\varepsilon_N} r_N) + C_{(2N-1)m} Y_m(k\sqrt{\varepsilon_N} r_N) \right] \cos m\varphi = \\ & = \sum_{m=-\infty}^{+\infty} (-i)^m A_m J_m(kr_N) \cos m\varphi + \sum_{m=-\infty}^{+\infty} C_{2Nm} H_m^{(2)}(kr_N) \cos m\varphi \\ & \sqrt{\varepsilon_N} \sum_{m=-\infty}^{+\infty} \left[C_{(2N-2)m} J'_m(k\sqrt{\varepsilon_N} r_N) + C_{(2N-1)m} Y'_m(k\sqrt{\varepsilon_N} r_N) \right] \cos m\varphi = \\ & = \sum_{m=-\infty}^{+\infty} (-i)^m A_m J'_m(kr_N) \cos m\varphi + \sum_{m=-\infty}^{+\infty} C_{2Nm} H_m^{(2)'}(kr_N) \cos m\varphi \end{aligned} \right. \quad (3.128)$$

Because of the completeness and orthogonality of the functions $\cos m\varphi$ the required vector of coefficients $C_m = \{C_{km}\}$, $k=1, 2N$, for any m is expressed through a system of linear algebraic equations:

$$A_m C_m = B_m, \quad (3.129)$$

where (see equation (3.130) on the next page)

$$B_m = \begin{pmatrix} 0 \\ 0 \\ \vdots \\ 0 \\ (-i)^m A_m J_m(kR) \\ (-i)^m A_m J'_m(kR) \end{pmatrix}. \quad (3.131)$$

The system of equations with the size $2N \times 2N$ is solved for all m -th coefficients of the expansion into a series of cylindrical functions (3.113)–(3.115). The resulting coefficients are then substituted into equation (3.113)–(3.115).

TM-polarization

The solution to the problem of diffraction of a plane TM-polarized electromagnetic waves on a multilayer dielectric cylinder is analogous to that in the case of TE-polarization, which was reviewed in the previous section. For TM-polarization we introduce the notation $H_z = \psi$. The boundary conditions take the form:

$$\left\{ \begin{array}{l} \psi_{1j} \Big|_{r_j} = \psi_{1(j+1)} \Big|_{r_j} \\ \frac{1}{\varepsilon_j} \frac{\partial \psi_{1j}}{\partial r} \Big|_{r_j} = \frac{1}{\varepsilon_{j+1}} \frac{\partial \psi_{1(j+1)}}{\partial r} \Big|_{r_j} \end{array} \right., \quad j = \overline{1, N-1}, \quad (3.132)$$

$$\left\{ \begin{array}{l} \psi_{1N} \Big|_R = \psi_2 \Big|_R \\ \frac{1}{\varepsilon_N} \frac{\partial \psi_{1N}}{\partial r} \Big|_R = \frac{\partial \psi_2}{\partial r} \Big|_R \end{array} \right. .$$

Here $r_N = R$.

Guided by the above described manner, it is easy to obtain the matrix of the system of equations (3.113)–(3.115), (3.132) (see equation (3.133) on the next page), similar to the matrix (3.130).

$$\begin{aligned}
 A_m = & \left(\begin{array}{cccc}
 J_m(k\sqrt{\varepsilon_1 r_1}) & -J_m(k\sqrt{\varepsilon_2 r_1}) & -Y_m(k\sqrt{\varepsilon_2 r_1}) & \\
 J'_m(k\sqrt{\varepsilon_1 r_1})\sqrt{\varepsilon_1} & -J'_m(k\sqrt{\varepsilon_2 r_1})\sqrt{\varepsilon_2} & -Y'_m(k\sqrt{\varepsilon_2 r_1})\sqrt{\varepsilon_2} & \\
 J_m(k\sqrt{\varepsilon_2 r_2}) & J_m(k\sqrt{\varepsilon_2 r_2}) & Y_m(k\sqrt{\varepsilon_2 r_2}) & -Y_m(k\sqrt{\varepsilon_3 r_2}) \\
 J'_m(k\sqrt{\varepsilon_2 r_2})\sqrt{\varepsilon_2} & J'_m(k\sqrt{\varepsilon_2 r_2})\sqrt{\varepsilon_2} & Y'_m(k\sqrt{\varepsilon_2 r_2})\sqrt{\varepsilon_2} & -J'_m(k\sqrt{\varepsilon_3 r_2})\sqrt{\varepsilon_3} \\
 \dots & \dots & \dots & \dots \\
 J_m(k\sqrt{\varepsilon_j r_j}) & J_m(k\sqrt{\varepsilon_j r_j}) & Y_m(k\sqrt{\varepsilon_j r_j}) & -Y_m(k\sqrt{\varepsilon_{j+1} r_j}) \\
 J'_m(k\sqrt{\varepsilon_j r_j})\sqrt{\varepsilon_j} & J'_m(k\sqrt{\varepsilon_j r_j})\sqrt{\varepsilon_j} & Y'_m(k\sqrt{\varepsilon_j r_j})\sqrt{\varepsilon_j} & -J'_m(k\sqrt{\varepsilon_{j+1} r_j})\sqrt{\varepsilon_{j+1}} \\
 \dots & \dots & \dots & \dots \\
 J_m(k\sqrt{\varepsilon_{N-1} r_{N-1}}) & J_m(k\sqrt{\varepsilon_{N-1} r_{N-1}}) & Y_m(k\sqrt{\varepsilon_{N-1} r_{N-1}}) & Y_m(k\sqrt{\varepsilon_N r_{N-1}}) \\
 J'_m(k\sqrt{\varepsilon_{N-1} r_{N-1}})\sqrt{\varepsilon_{N-1}} & J'_m(k\sqrt{\varepsilon_{N-1} r_{N-1}})\sqrt{\varepsilon_{N-1}} & Y'_m(k\sqrt{\varepsilon_{N-1} r_{N-1}})\sqrt{\varepsilon_{N-1}} & -Y'_m(k\sqrt{\varepsilon_N r_{N-1}})\sqrt{\varepsilon_N} \\
 & & J_m(k\sqrt{\varepsilon_N r_N}) & -H_m^{(2)}(kr_N) \\
 & & J'_m(k\sqrt{\varepsilon_N r_N})\sqrt{\varepsilon_N} & -H_m^{(2)'}(kr_N)
 \end{array} \right), \tag{3.130}
 \end{aligned}$$

$$\left(\begin{array}{cccc}
J_m(k\sqrt{\varepsilon_1 r_1}) & -J_m(k\sqrt{\varepsilon_2 r_1}) & -Y_m(k\sqrt{\varepsilon_2 r_1}) & \\
J'_m(k\sqrt{\varepsilon_1 r_1}) \frac{1}{\sqrt{\varepsilon_1}} & -J'_m(k\sqrt{\varepsilon_2 r_1}) \frac{1}{\sqrt{\varepsilon_2}} & -Y'_m(k\sqrt{\varepsilon_2 r_1}) \frac{1}{\sqrt{\varepsilon_2}} & \\
J_m(k\sqrt{\varepsilon_2 r_2}) & J_m(k\sqrt{\varepsilon_2 r_2}) & Y_m(k\sqrt{\varepsilon_2 r_2}) & -Y_m(k\sqrt{\varepsilon_3 r_2}) \\
J'_m(k\sqrt{\varepsilon_2 r_2}) \frac{1}{\sqrt{\varepsilon_2}} & J'_m(k\sqrt{\varepsilon_2 r_2}) \frac{1}{\sqrt{\varepsilon_2}} & Y'_m(k\sqrt{\varepsilon_2 r_2}) \frac{1}{\sqrt{\varepsilon_2}} & -Y'_m(k\sqrt{\varepsilon_3 r_2}) \frac{1}{\sqrt{\varepsilon_3}} \\
\vdots & \vdots & \vdots & \vdots \\
J_m(k\sqrt{\varepsilon_j r_j}) & J_m(k\sqrt{\varepsilon_j r_j}) & Y_m(k\sqrt{\varepsilon_j r_j}) & -Y_m(k\sqrt{\varepsilon_{j+1} r_j}) \\
J'_m(k\sqrt{\varepsilon_j r_j}) \frac{1}{\sqrt{\varepsilon_j}} & J'_m(k\sqrt{\varepsilon_j r_j}) \frac{1}{\sqrt{\varepsilon_j}} & Y'_m(k\sqrt{\varepsilon_j r_j}) \frac{1}{\sqrt{\varepsilon_j}} & -Y'_m(k\sqrt{\varepsilon_{j+1} r_j}) \frac{1}{\sqrt{\varepsilon_{j+1}}} \\
\vdots & \vdots & \vdots & \vdots \\
J_m(k\sqrt{\varepsilon_{N-1} r_{N-1}}) & J_m(k\sqrt{\varepsilon_{N-1} r_{N-1}}) & Y_m(k\sqrt{\varepsilon_{N-1} r_{N-1}}) & Y_m(k\sqrt{\varepsilon_N r_{N-1}}) \\
J'_m(k\sqrt{\varepsilon_{N-1} r_{N-1}}) \frac{1}{\sqrt{\varepsilon_{N-1}}} & J'_m(k\sqrt{\varepsilon_{N-1} r_{N-1}}) \frac{1}{\sqrt{\varepsilon_{N-1}}} & Y'_m(k\sqrt{\varepsilon_{N-1} r_{N-1}}) \frac{1}{\sqrt{\varepsilon_{N-1}}} & -Y'_m(k\sqrt{\varepsilon_N r_{N-1}}) \frac{1}{\sqrt{\varepsilon_N}} \\
& & J_m(k\sqrt{\varepsilon_N r_N}) & -H_m^{(2)}(kr_N) \\
& & J'_m(k\sqrt{\varepsilon_N r_N}) \frac{1}{\sqrt{\varepsilon_N}} & -H_m^{(2)}(kr_N)
\end{array} \right) \tag{3.133}$$

$$\tilde{b}_{2N} = b_{2N} - \left(a_{2N,2N-1} - a_{2N,2N-2} \frac{\tilde{a}_{2(N-1),2N-1}}{\tilde{a}_{2(N-1),2(N-1)}} \right) \frac{b_{2N-1}}{\tilde{a}_{2N-1,2N-1}}.$$

With the reverse course it is possible to obtain an expression for solving systems of linear equations:

$$\begin{aligned} c_{2N} &= \frac{\tilde{b}_{2N}}{\tilde{a}_{2N,2N}}, \\ c_{2N-1} &= \left(b_{2N-1} - a_{2N-1,2N} c_{2N} \right) \frac{1}{\tilde{a}_{2N-1,2N-1}}, \\ c_{2(N-i)} &= -c_{2(N-i)+1} \frac{\tilde{a}_{2(N-i),2(N-i)+1}}{\tilde{a}_{2(N-i),2(N-i)}}, \\ c_{2(N-i)-1} &= - \left(a_{2(N-i)-1,2(N-i)} c_{2(N-i)} + a_{2(N-i)-1,2(N-i)+1} c_{2(N-i)+1} \right) \frac{1}{\tilde{a}_{2(N-i)-1,2(N-i)-1}}. \end{aligned} \quad (3.137)$$

Here $i = \overline{1, N-1}$, and in the latter of equations (3.137) at $i = N-1$:

$$\tilde{a}_{2(N-i)-1,2(N-i)-1} = a_{11}.$$

Raleigh series in ascending integer indices represent the diffracted field in the form of an infinite set of multipoles, and in this set the number of important terms increases with the increase of the ratio of the transverse dimension of the body to the wavelength. The smaller $k\sqrt{\varepsilon_i r_i}$, the more rapidly series converges. Accordingly, the diffraction field for small $k\sqrt{\varepsilon_i r_i}$ has a relatively simple form and becomes more complicated with the increase of $k\sqrt{\varepsilon_i r_i}$. The rapid decrease of the terms of the series, starting with the numbers $m \sim k\sqrt{\varepsilon_i r_i}$, enables us to ignore the remainder of the series, even for large values of $k\sqrt{\varepsilon_i r_i}$.

However, for very large values of $k\sqrt{\varepsilon_i r_i}$ the summation is difficult because of the very long computing time. The transition to the Watson series is effective [1].

3.3.2. The analytical solution for a two-layer cylinder

Study [1] gives an analytic solution of the two-dimensional problem of diffraction of a plane electromagnetic monochromatic wave of TE-/TM-polarization on a homogeneous dielectric circular cylinder. Using the method proposed in section 3.3.1 we obtain an analytic solution of the problem of diffraction of an arbitrary electromagnetic wave on a two-layer dielectric circular cylinder, where the layers are represented in the form of a rod and a shell (Fig. 3.26).

The system of equations (3.113)–(3.115) reduces to:

$$\begin{aligned}\psi_{11} &= \sum_{m=-\infty}^{+\infty} C_{1m} J_m(k\sqrt{\varepsilon_1}r) \cos m\varphi, \quad 0 \leq r \leq r_1; \\ \psi_{12} &= \sum_{m=-\infty}^{+\infty} \left[C_{2m} J_m(k\sqrt{\varepsilon_2}r) + C_{3m} Y_m(k\sqrt{\varepsilon_2}r) \right] \cos m\varphi, \quad r_1 < r \leq r_2; \quad (3.138) \\ \psi_2 &= \psi_0 + \sum_{m=-\infty}^{+\infty} C_{4m} H_m^{(2)}(kr) \cos m\varphi, \quad r > r_2.\end{aligned}$$

The problem is reduced to finding the unknown coefficients C_{1m} , C_{2m} , C_{3m} , C_{4m} . Further, similarly to the case of the N -layered cylinder, as described in Section 3.3.1, we obtain a system of four linear algebraic equations with four unknowns. It is not difficult to solve analytically such a system is not difficult, so here are only the results are presented.

TE-polarization

$$\begin{aligned}C_{1m} &= \frac{(-i)^m A_m \sqrt{\varepsilon_2} \left(J_m(k\sqrt{\varepsilon_2}r_1) Y'_m(k\sqrt{\varepsilon_2}r_1) - J'_m(k\sqrt{\varepsilon_2}r_1) Y_m(k\sqrt{\varepsilon_2}r_1) \right)}{\Delta} \\ &\quad \cdot \frac{\left(H_m^{(2)}(kr_2) J_m(kr_2) - H_m^{(2)}(kr_2) J'_m(kr_2) \right)}{\Delta}, \\ C_{2m} &= \frac{(-i)^m A_m \left(Y_m(k\sqrt{\varepsilon_2}r_1) J'_m(k\sqrt{\varepsilon_1}r_1) \sqrt{\varepsilon_1} - Y'_m(k\sqrt{\varepsilon_2}r_1) \sqrt{\varepsilon_2} J_m(k\sqrt{\varepsilon_1}r_1) \right)}{\Delta} \\ &\quad \cdot \frac{\left(H_m^{(2)}(kr_2) J'_m(kr_2) - H_m^{(2)}(kr_2) J_m(kr_2) \right)}{\Delta}, \\ C_{3m} &= \frac{(-i)^m A_m \left(J'_m(k\sqrt{\varepsilon_2}r_1) \sqrt{\varepsilon_2} J_m(k\sqrt{\varepsilon_1}r_1) - J_m(k\sqrt{\varepsilon_2}r_1) J'_m(k\sqrt{\varepsilon_1}r_1) \sqrt{\varepsilon_1} \right)}{\Delta} \\ &\quad \cdot \frac{\left(H_m^{(2)}(kr_2) J'_m(kr_2) - H_m^{(2)}(kr_2) J_m(kr_2) \right)}{\Delta},\end{aligned}$$

$$\begin{aligned}
C_{4m} = & (-i)^m A_m \left[\left(Y_m(k\sqrt{\varepsilon_2}r_1) J'_m(k\sqrt{\varepsilon_1}r_1) \sqrt{\varepsilon_1} - Y'_m(k\sqrt{\varepsilon_2}r_1) \sqrt{\varepsilon_2} J_m(k\sqrt{\varepsilon_1}r_1) \right) \cdot \right. \\
& \cdot \left(J_m(k\sqrt{\varepsilon_2}r_2) J'_m(kr_2) - J'_m(k\sqrt{\varepsilon_2}r_2) \sqrt{\varepsilon_2} J_m(kr_2) \right) + \\
& + \left(J'_m(k\sqrt{\varepsilon_2}r_1) \sqrt{\varepsilon_2} J_m(k\sqrt{\varepsilon_1}r_1) - J_m(k\sqrt{\varepsilon_2}r_1) J'_m(k\sqrt{\varepsilon_1}r_1) \sqrt{\varepsilon_1} \right) \cdot \\
& \cdot \left. \left(Y_m(k\sqrt{\varepsilon_2}r_2) J'_m(kr_2) - Y'_m(k\sqrt{\varepsilon_2}r_2) \sqrt{\varepsilon_2} J_m(kr_2) \right) \right] / \Delta
\end{aligned}$$

Here

$$\begin{aligned}
\Delta = & \left(Y_m(k\sqrt{\varepsilon_2}r_1) J'_m(k\sqrt{\varepsilon_1}r_1) \sqrt{\varepsilon_1} - Y'_m(k\sqrt{\varepsilon_2}r_1) \sqrt{\varepsilon_2} J_m(k\sqrt{\varepsilon_1}r_1) \right) \cdot \\
& \left(J'_m(k\sqrt{\varepsilon_2}r_2) \sqrt{\varepsilon_2} H_m^{(2)}(kr_2) - J_m(k\sqrt{\varepsilon_2}r_2) H_m^{(2)}(kr_2) \right) + \\
& + \left(J'_m(k\sqrt{\varepsilon_2}r_1) \sqrt{\varepsilon_2} J_m(k\sqrt{\varepsilon_1}r_1) - J_m(k\sqrt{\varepsilon_2}r_1) J'_m(k\sqrt{\varepsilon_1}r_1) \sqrt{\varepsilon_1} \right) \cdot \\
& \cdot \left(Y'_m(k\sqrt{\varepsilon_2}r_2) \sqrt{\varepsilon_2} H_m^{(2)}(kr_2) - Y_m(k\sqrt{\varepsilon_2}r_2) H_m^{(2)}(kr_2) \right)
\end{aligned}$$

The calculated coefficients are substituted into (3.138).

TM-polarization

$$\begin{aligned}
C_{1m} = & \frac{(-i)^m A_m \frac{1}{\sqrt{\varepsilon_2}} \left(J_m(k\sqrt{\varepsilon_2}r_1) Y'_m(k\sqrt{\varepsilon_2}r_1) - J'_m(k\sqrt{\varepsilon_2}r_1) Y_m(k\sqrt{\varepsilon_2}r_1) \right)}{\Delta} \\
& \cdot \frac{\left(H_m^{(2)}(kr_2) J_m(kr_2) - H_m^{(2)}(kr_2) J'_m(kr_2) \right)}{\Delta}, \\
C_{2m} = & \frac{(-i)^m A_m \left(Y_m(k\sqrt{\varepsilon_2}r_1) J'_m(k\sqrt{\varepsilon_1}r_1) \frac{1}{\sqrt{\varepsilon_1}} - Y'_m(k\sqrt{\varepsilon_2}r_1) J_m(k\sqrt{\varepsilon_1}r_1) \frac{1}{\sqrt{\varepsilon_2}} \right)}{\Delta} \\
& \cdot \frac{\left(H_m^{(2)}(kr_2) J'_m(kr_2) - H_m^{(2)}(kr_2) J_m(kr_2) \right)}{\Delta}, \\
C_{3m} = & \frac{(-i)^m A_m \left(J'_m(k\sqrt{\varepsilon_2}r_1) J_m(k\sqrt{\varepsilon_1}r_1) \frac{1}{\sqrt{\varepsilon_2}} - J_m(k\sqrt{\varepsilon_2}r_1) J'_m(k\sqrt{\varepsilon_1}r_1) \frac{1}{\sqrt{\varepsilon_1}} \right)}{\Delta} \\
& \cdot \frac{\left(H_m^{(2)}(kr_2) J'_m(kr_2) - H_m^{(2)}(kr_2) J_m(kr_2) \right)}{\Delta},
\end{aligned}$$

$$\begin{aligned}
C_{4m} = & (-i)^m A_m \left[\left(Y_m(k\sqrt{\varepsilon_2}r_1) J'_m(k\sqrt{\varepsilon_1}r_1) \frac{1}{\sqrt{\varepsilon_1}} - Y'_m(k\sqrt{\varepsilon_2}r_1) J_m(k\sqrt{\varepsilon_1}r_1) \frac{1}{\sqrt{\varepsilon_2}} \right) \cdot \right. \\
& \cdot \left(J_m(k\sqrt{\varepsilon_2}r_2) J'_m(kr_2) - J'_m(k\sqrt{\varepsilon_2}r_2) J_m(kr_2) \frac{1}{\sqrt{\varepsilon_2}} \right) + \\
& + \left. \left(J'_m(k\sqrt{\varepsilon_2}r_1) J_m(k\sqrt{\varepsilon_1}r_1) \frac{1}{\sqrt{\varepsilon_2}} - J_m(k\sqrt{\varepsilon_2}r_1) J'_m(k\sqrt{\varepsilon_1}r_1) \frac{1}{\sqrt{\varepsilon_1}} \right) \right] \cdot \\
& \cdot \left. \left(Y_m(k\sqrt{\varepsilon_2}r_2) J'_m(kr_2) - Y'_m(k\sqrt{\varepsilon_2}r_2) J_m(kr_2) \frac{1}{\sqrt{\varepsilon_2}} \right) \right] / \Delta
\end{aligned}$$

Here

$$\begin{aligned}
\Delta = & \left(Y_m(k\sqrt{\varepsilon_2}r_1) Y'_m(k\sqrt{\varepsilon_1}r_1) \frac{1}{\sqrt{\varepsilon_1}} - J'_m(k\sqrt{\varepsilon_2}r_1) J_m(k\sqrt{\varepsilon_1}r_1) \frac{1}{\sqrt{\varepsilon_2}} \right) \cdot \\
& \left(J'_m(k\sqrt{\varepsilon_2}r_2) H_m^{(2)}(kr_2) \frac{1}{\sqrt{\varepsilon_2}} - J_m(k\sqrt{\varepsilon_2}r_2) H_m^{(2)}(kr_2) \right) + \\
& + \left(J'_m(k\sqrt{\varepsilon_2}r_1) J_m(k\sqrt{\varepsilon_1}r_1) \frac{1}{\sqrt{\varepsilon_2}} - J_m(k\sqrt{\varepsilon_2}r_1) J'_m(k\sqrt{\varepsilon_1}r_1) \frac{1}{\sqrt{\varepsilon_1}} \right) \cdot \\
& \cdot \left(Y'_m(k\sqrt{\varepsilon_2}r_2) H_m^{(2)}(kr_2) \frac{1}{\sqrt{\varepsilon_2}} - Y_m(k\sqrt{\varepsilon_2}r_2) H_m^{(2)}(kr_2) \right)
\end{aligned}$$

The calculated coefficients are substituted into (3.138).

In the equations for the coefficients C_{km} , $k = \overline{1,4}$, the constants A_m are found from (3.127) and characterize the incident light wave.

3.3.3. Diffraction on a gradient microlens Diffraction of electromagnetic waves on the internal Luneberg lens

Consider the diffraction of a plane TE-polarized electromagnetic wave with a length $\lambda = 1 \mu\text{m}$ on a dielectric cylinder of radius $R = 1 \mu\text{m}$, whose refractive index depends on the radius as follows (the inner Luneberg lens) [68]:

$$n^2(r) = \frac{1+r_1^2-r^2}{r_1^2}, \quad r_1 \leq 1, \quad (3.139)$$

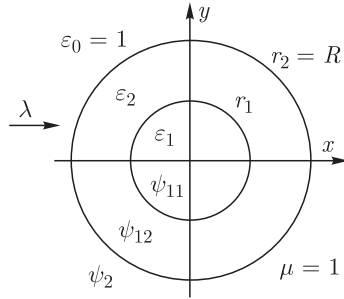


Fig. 3.26. The two-layer dielectric cylinder.

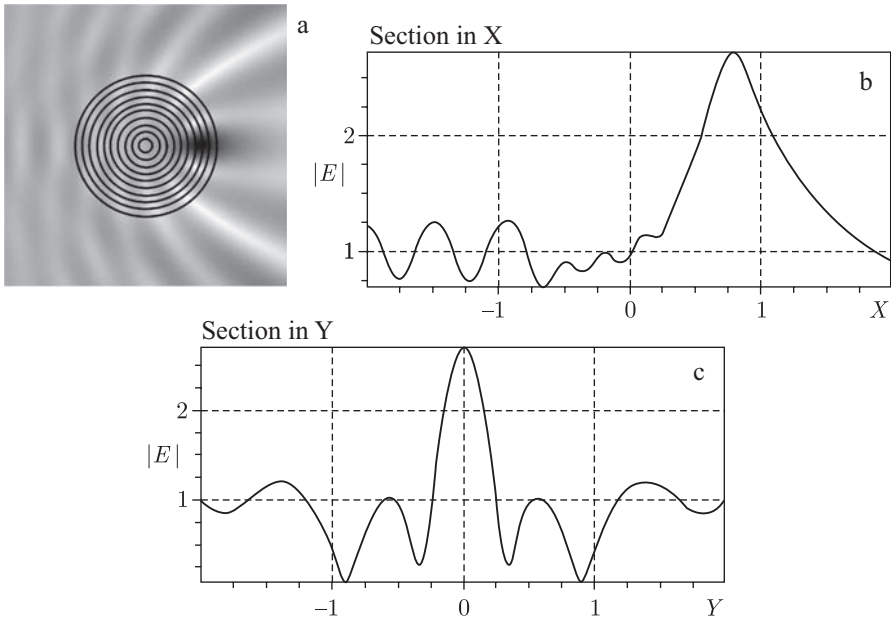


Fig. 3.27. Distribution of electric field amplitude: a) 2D distribution, b) the section on the X axis (horizontal axis) through the focus, c) cross-section on the Y axis (vertical axis) through the focus.

where r_1 is the distance from the centre of the cylinder to the point of the geometrical focus. As an example, consider $r_1 = 0.75 \mu\text{m}$. We select the number of layers of the cylinder equal to 10 and the maximum order of approximating Bessel functions in the series (3.113)–(3.115) as 20.

The amplitude distribution of the projection of the vector of the strength of electric field $E_z(x, y)$ is shown in Fig. 3.27.

The total size of the diffraction pattern is $4 \times 4 \text{ mm}$ (Fig. 3.27a). The number of counts of the sampling grid was 300×300 pixels. The value of the focal length r_1 , calculated using the above described method, is $r_1 \approx 0.787 \text{ mm}$. The relative

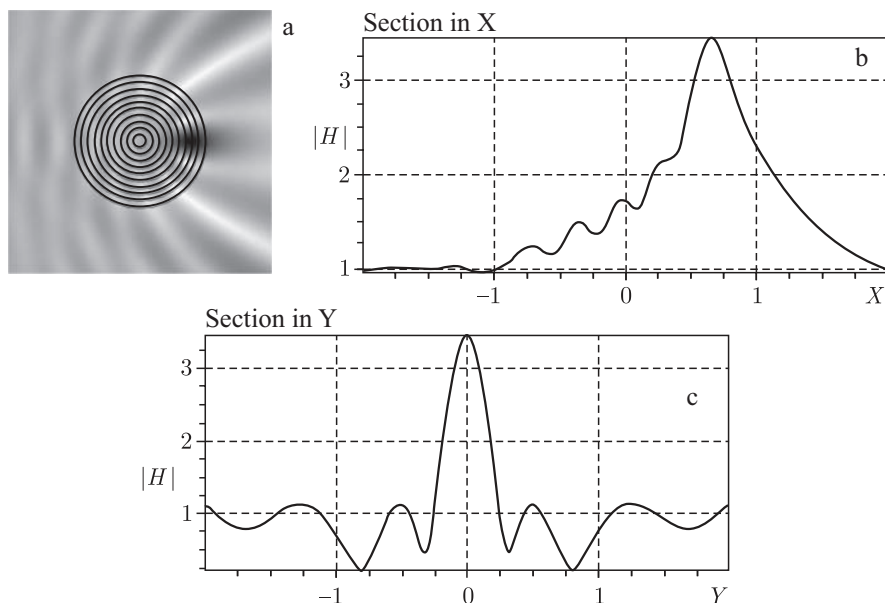


Fig. 3.28. The amplitude distribution of the magnetic field: a) 2D distribution, b) the section on the X axis (horizontal axis) through the focus, c) cross-section in Y axis (vertical axis) through the focus.

error in comparison with the specified value r_1 is $\approx 4.9\%$. It should be noted that the calculated value r_1 is compared with the value obtained for ray approximation.

Consider the problem with the same parameters, but for the case of a TM-polarized incident plane wave.

The amplitude distribution of the magnetic field is shown in Fig.3.28.

The value of the focal length r_1 was $r_1 \approx 0.653 \mu\text{m}$. The relative deviation of the calculated focal length from the given value of r_1 is $\approx 12.9\%$.

The study of diffraction of light on the Luneberg lens, whose dimensions are comparable with the incident electromagnetic wave, with the developed method was carried out in a series of numerical experiments. The main task was to check how many layers of the lens will be sufficient to obtain a stable value of the focal length, and compare it with the prescribed value, which was used for calculations by the beam approximation of the refractive index of the lens.

The following parameters of the diffraction pattern were chosen: the size $4 \times 4 \mu\text{m}$, number of samples 400×400 pixels, the outer radius of the cylinder $1 \mu\text{m}$, the prescribed focal length $0.5 \mu\text{m}$.

Based on the results it was concluded that for the wavelengths comparable to the size of the Luneberg lens about 30–40 layers, approximating the lens, are sufficient. Moreover, the deviation of the calculated focal distance from the specified value of the focal length, obtained using the ray approximation, is no more than 10%.

It was also interesting to know the magnitude of the intensity at the focus of the Luneberg lens, and how it changes depending on the number of approximating

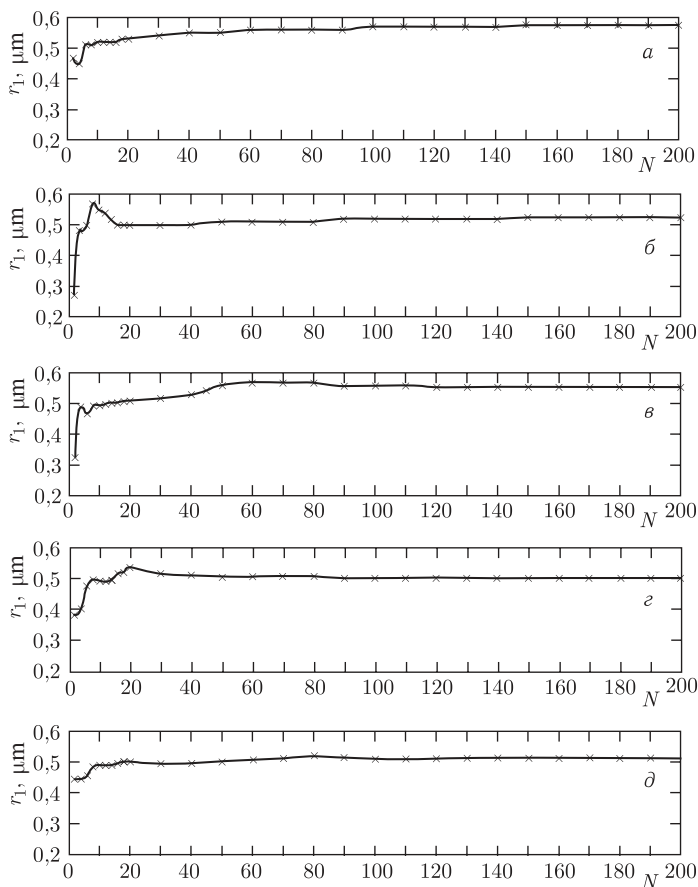


Fig. 3.29. Dependence of the focal length of the Luneberg lens on the number of layers of the cylinder at different wavelengths of the incident wave: a) $\lambda = 1 \mu\text{m}$; b) $\lambda = 0.8 \mu\text{m}$, c) $\lambda = 0.6 \mu\text{m}$, d) $\lambda = 0.4 \mu\text{m}$, e) $\lambda = 0.2 \mu\text{m}$.

segments. The dependences obtained for fixed values of the length of the incident wave are shown in Fig. 3.30.

Based on the numerical results, it is concluded that the developed method provides a stable solution for a given wavelength. It should be noted that with decreasing wavelength the intensity at the focus increases. This is because decreasing wavelength the diffraction effects become weaker, and the light concentrates more and more at the focus. It can be assumed that with a further decrease in wavelength, when the ray approximation holds, the intensity of the focus will tend to 200, and this is the number of pixels placed on the diameter of the circle, and each pixel corresponds to a beam which should theoretically pass through the focus of the Luneberg lens.

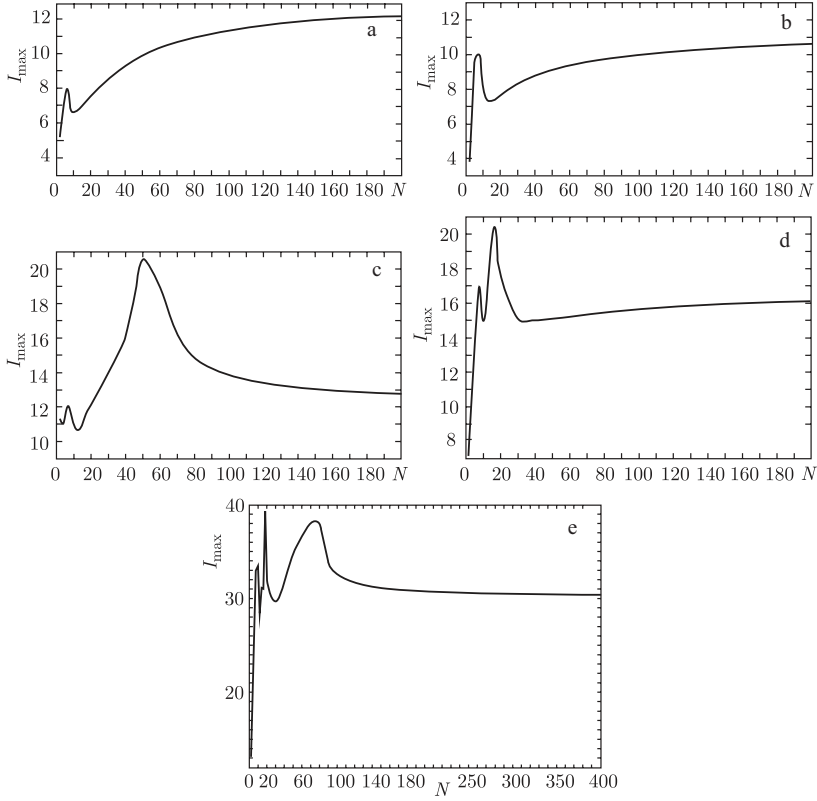


Fig. 3.30. Dependence of the intensity at the focus of the Luneberg lens on the number of layers of the cylinder at different wavelengths of the incident wave: a) $\lambda = 1 \mu\text{m}$; b) $\lambda = 0.8 \mu\text{m}$; c) $\lambda = 0.6 \mu\text{m}$; d) $\lambda = 0.4 \mu\text{m}$; e) $\lambda = 0.2 \mu\text{m}$.

Diffraction of electromagnetic waves on a generalized Luneberg lens

Consider the case where $r_1 > 1$. The refractive index of the generalized Luneberg lens is written as [68]:

$$n(r) = \exp \left[\frac{1}{\pi} \int_{\rho}^1 \frac{\arcsin(h/r_1) dh}{\sqrt{h^2 - \rho^2}} \right], \quad \rho = n(r)r, \quad 0 < \rho < 1. \quad (3.140)$$

The transcendental equation (3.140) was solved numerically with respect to $n(r)$, since the integral in (3.140) is not taken in elementary functions. Let us assume that a flat TE-polarized electromagnetic wave with a wavelength of $\lambda = 0.2 \mu\text{m}$ falls on a dielectric cylinder. The focal length is chosen equal to $\lambda = 2.55 \mu\text{m}$, the radius of the lens is $R = 1 \mu\text{m}$. We define the number of layers of the cylinder equal to 100 and the maximum order of the approximating cylinder functions as 35.

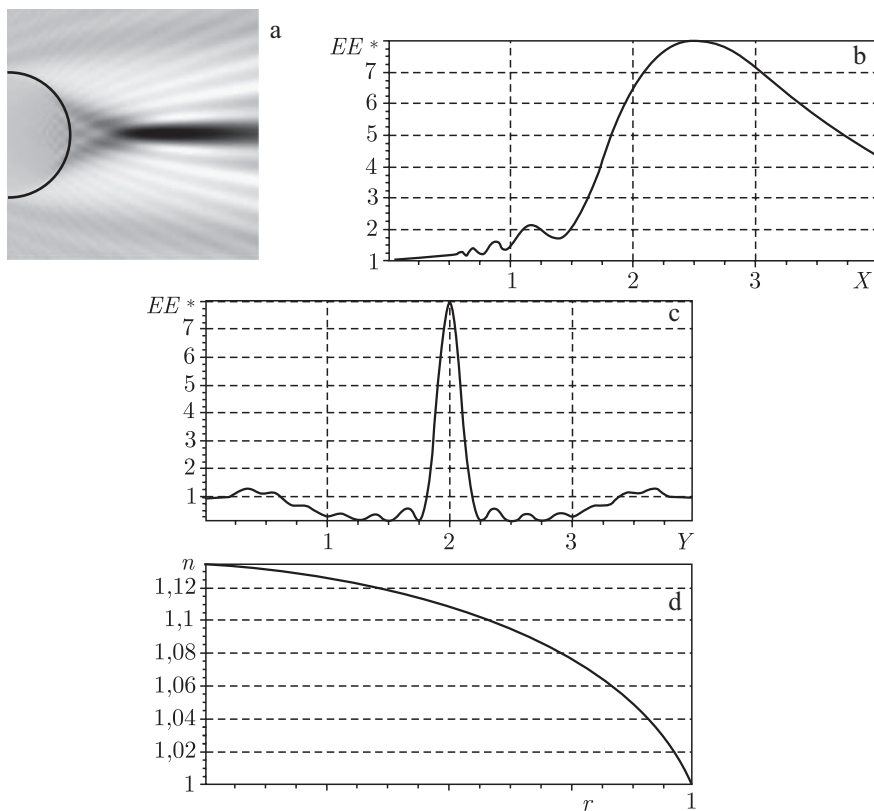


Fig. 3.31. The distribution of the intensity of the electric field: a) 2D distribution, b) the section on the X axis (horizontal axis) through the focus, c) cross-section on the Y axis (vertical axis) through the focus, d) the dependence of the refractive index of the lens on the radial coordinate.

The distribution of the intensity of the electric field is shown in Fig. 3.31:

The total size of the diffraction pattern 4×4 mm. The number of counts??? on the sampling grid 400×400 . The value of the focal length r_1 , calculated using the above described method, was $r_1 \approx 2.48 \mu\text{m}$. The relative error in comparison with the specified value r_1 was equal to $\approx 3\%$.

Consider the same case, but for a TM-polarized plane electromagnetic wave.

The intensity distribution of the magnetic field is shown in Fig.3.32.

The total size of the diffraction pattern was 4×4 mm. The number of counts??? on the sampling grid 400×400 . The value of the focal length r_1 , calculated using the above described method, was $r_1 \approx 2.5 \mu\text{m}$. The relative error in comparison with the specified value r_1 was equal to $\approx 2\%$.

In all these cases the dependence of the refractive index of the radius decreases monotonically from the centre of the circle to the surface (at a distance of $1 \mu\text{m}$ from the centre of the refractive index is equal to 1). In the case of the generalized Luneberg lens(3.140), the refractive index at the centre of the circle is $n \approx 1.134$